Acidity of aerosol particles: Estimation based on a chemical thermodynamic model and development of a direct measurement method

（エアロゾル粒子の酸性度：化学熱力学モデルに基づいた推定および直接測定法の開発）

SONG Qinping
宋 秦平

A dissertation for the degree of Doctor of Science
Department of Earth and Environmental Sciences,
Graduate School of Environmental Studies, Nagoya University
（名古屋大学大学院環境学研究科地球環境科学専攻学位論文 博士（理学））

2021

Abstract

Aerosol particles are suspended solid or liquid particles in the atmosphere that impact many chemical and physical processes and human health. Aerosol particles consist of various substances including hygroscopic components such as sulfate, nitrate and ammonium. Depending on relative humidity (RH) of the air, aerosol particles absorb water vapor and grow their size. Thus, the aerosol particles often contain liquid water of high ionic strength. Aerosol acidity is the pH of the liquid water in the aerosol particles. It is a critical parameter that strongly affects the gas/particle phase partitioning of inorganic semivolatile species and the multiphase chemical processes. However, it is difficult to measure aerosol pH directly because of small solution quantity and the high ionic strength of atmospheric aerosol particles. In the earlier studies, aerosol pH is inferred based on the aerosol sample extracts, but it cannot adequately indicate real aerosol pH due to much lower ionic strength of extracts than that in aerosols. Recently, the chemical thermodynamic models are often used to estimate aerosol pH during short-term and high concentration events in some areas. However, long-term studies based on a high-quality data set including gaseous ammonia are scarce.

In this study, aerosol pH is estimated by using a benchmark chemical thermodynamic model, the Extended Aerosol Inorganics Model (E-AIM), based on two-years data obtained from continuous observations of water-soluble gaseous species (NH_3 and HNO_3) and ionic constituents of particles in Nagoya during 2017–2018. Moreover, based on the same data, the factors affecting aerosol pH are investigated by various sensitivity tests conducted using E-AIM model. The estimation results show that aerosol pH presented a seasonal variation of low in summer (an average of 2.31 ± 0.39) and high in winter (an average of 3.05 ± 0.15). The sensitivity test results indicate that (1) such seasonal variation of aerosol pH appears only in the low SO_4^{2-} concentration area like Nagoya, (2) the liquid water content of aerosol particles is related to temperature, resulting in the influence of temperature on aerosol pH, and (3) ammonium, which can neutralize SO_4^{2-}, is also an important driving factor for aerosol pH.

In order to provide comparable data for relating the chemical thermodynamic estimations with atmospheric aerosol particles, a direct measurement method of aerosol pH is needed. Herein, according to hygroscopic equilibrium under high RH conditions, a direct measurement method for the pH of hygroscopic particles was developed by utilizing a pH testing paper. The color response accuracy for 6 kinds of pH testing papers were examined under various ionic strengths to select the best performing paper under higher ionic strength of various salt mixtures. Then the KNO_3 saturated solution is used to provide the constant RH at 92%, enabling hygroscopic constituents in the aerosol sample to form an aqueous droplet which has realistic high ionic strength in the atmosphere. After selected the best pH test paper using the droplet tests, it is further examined for the measurement capability of atmospheric aerosols. The results indicate that this method needs more than about 12 μg per sample spot of fine aerosols to form the detectable size of the deliquesced droplet.

By comparing the measurement results of the pH testing paper method and the estimation results from the E-AIM model, the effect of gaseous NH_3 on the pH testing paper method was examined. The NH_3 concentration in the chamber should be controlled to obtain more reliable data. Moreover, this comparison also indicates that the pH definition based on a molality scale is the most suitable when the E-AIM model is used to estimate aerosol pH.

The results of this thesis revealed the seasonal variation and driving factors of aerosol pH in Nagoya, which is expected to be a representative for other less-polluted urban areas and a future situation for the currently polluted but improving areas. Furthermore, approaches shown in this study, including the application of E-AIM model and the pH testing paper method, can provide more realistic pH data on various acidity-dependent chemical processes on aerosol particles.

Contents

Chapter 1: Introduction

1.1 Atmospheric aerosol particle and its acidity

Aerosol particles are the suspension of fine solid or liquid particles in the atmosphere, arise from various anthropogenic activities and natural sources. It has a complex composition, including hygroscopic components such as sulfate, nitrate, and ammonium. These compounds enhance the hygroscopic ability of aerosol particles, resulting in particle growth with relative humidity (RH) by absorbing water vapor (Fig 1, Seinfeld and Pandis, 2016). At high RH condition, aerosol particles with high liquid water are ubiquitous and often in non-ideal state due to the high ionic strength (Mekic and Gligorovski, 2021; Wei et al., 2018). The hydrogen ion in the liquid phase of aerosol particle plays an important role in these atmospheric chemical reactions that impacts the gas/particle partitioning of semivolatile species (Guo et al., 2017a), the formation of secondary inorganic/organic aerosols (SIA and SOA) (Surratt et al., 2010, 2007; Sqizzato et al., 2013; Han et al., 2016), and the solubility of some metals (Meskhidze et al., 2005, 2003). Therefore, it has attracted increasing interest in aerosol research. Similar to aquatic chemistry, the hydrogen ion in the liquid phase of aerosol particles is defined as aerosol acidity (Fig. 2). To more clearly indicate aerosol acidity, the pH scale also uses in this field. It is calculated as the negative logarithm of H^+ ion activity in the liquid phase of aerosol particles and referred to as aerosol pH.

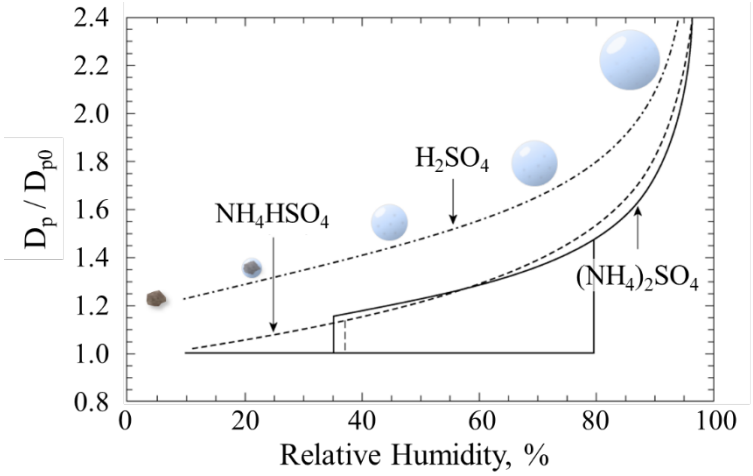

Figure 1. Illustration of diameter change of $(NH_4)_2SO_4$, NH_4HSO_4, and H_2SO_4 particles as a function of relative humidity. D_{p0} is the diameter of the particle at 0% RH.

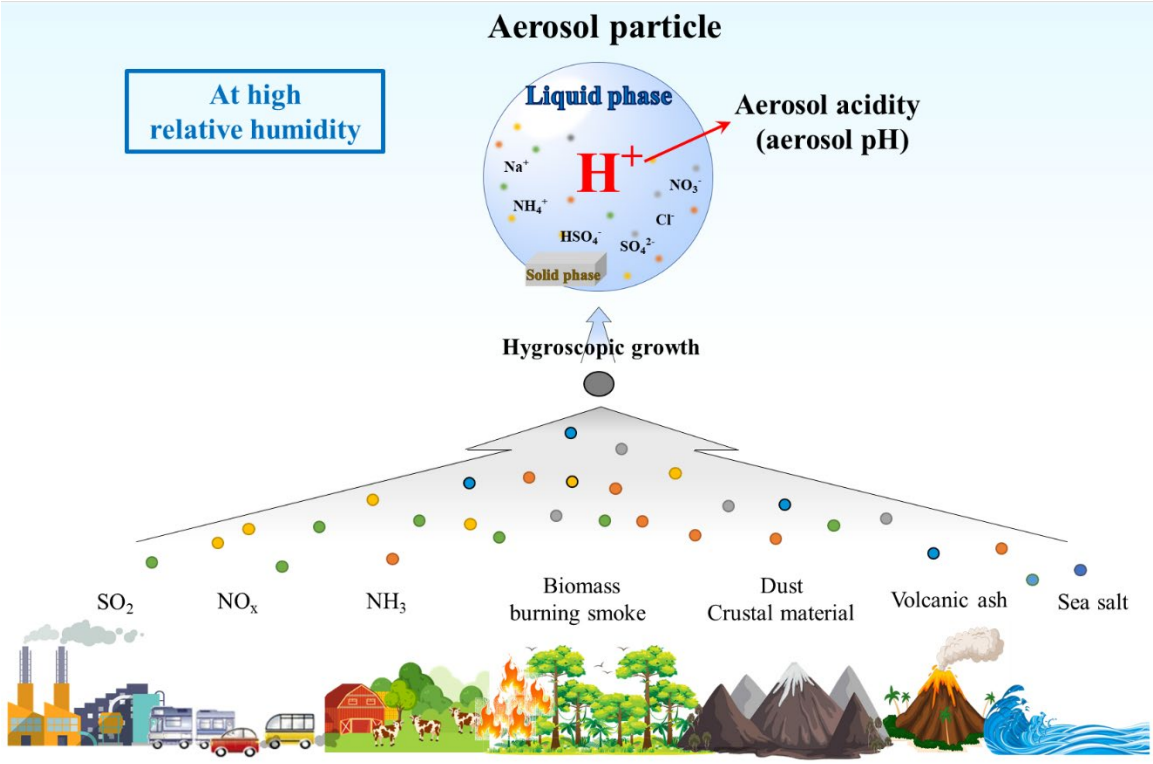

Figure 2. Schematic diagram of aerosol acidity. The aerosol particles form from various emission sources. At high relative humidity, the hygroscopic compounds in the aerosol particle grow the particle size by absorbing water vapor, forming the liquid phase of aerosol particle. The H^+ ion in the liquid phase is defined as aerosol acidity. The negative logarithm of its activity is referred to as aerosol pH.

1.2 Environmental effect of aerosol acidity

In the atmosphere, aerosol acidity directly affects the gas/particle partitioning of NH_3/NH_4^+, HNO_3/NO_3^-, HCl/Cl^-, and some organic acids and bases (Guo et al., 2017a; Ahrens et al., 2012). At lower aerosol acidity condition, the phase partitioning of total ammonium ($T\_NH_4^+ = NH_{3(g)} + NH_4^+{}_{(p)}$) tends to gaseous ammonia (NH_3) (Seinfeld and Pandis, 2016). With the increase of aerosol acidity, gaseous NH_3 decrease and NH_4^+ ion in the aerosol particle increases, resulting in extending $T\_NH_4^+$ atmospheric lifetime and lowering its relevant dry deposition velocity (Nenes et al., 2021). Similar to $T\_NH_4^+$, the phase partitioning of total nitrate ($T\_NO_3^- = HNO_{3(g)} + NO_3^-$) is also controlled by aerosol acidity. While, on the contrary, high aerosol acidity is helpful for forming gaseous nitric

acid (NHO_3), resulting in shortening $T\_NO_3^-$ atmospheric lifetime and slowing its deposition down (Seinfeld and Pandis, 2016; Nenes et al., 2021). Aerosol acidity therefore directly affects inorganic nitrogen deposition by governing the phase partitioning of $T\_NH_4^+$ and $T\_NO_3^-$, thereby affecting the ecosystem load of nitrogen (Bobbink et al., 2010).

In addition to the effect on nitrogen deposition, aerosol acidity controls acid deposition directly which can engender water acidification and the deterioration of soil and vegetation (Lawrence et al., 2015; Jia and Gao, 2017; Wu and Zhang, 2018). Aerosol acidity also strongly influences some important formation pathway of second organic aerosols (SOA), such as α-pinene and isoprene oxidation processes (Surratt et al., 2010, 2007; Han et al., 2016; Zhang et al., 2019). Results of laboratory chamber experiments and field measurements have indicated that high aerosol acidity engenders increased SOA formation (Jang et al., 2002; Iinuma et al., 2004; Rengarajan et al., 2011; Zhang et al., 2015). Previous studies about human health assessment also suggest that aerosol acidity is important for the solubilities of hazardous materials in aerosol particles (e.g., trace metals) (Deguillaume et al., 2005; Fang et al., 2017). Moreover, the high acidity of particles can affect the human respiratory system adversely by inhalation of the acidic particles directly (Dockery et al., 1996; Raizenne et al., 1996).

As a result, aerosol acidity is a critical parameter in atmospheric science. Obtaining the information of aerosol acidity is beneficial for many related studies (Su et al., 2020). For example, Nenes et al. (2021) indicated aerosol acidity is key to estimating the dry deposition and atmospheric lifetime of inorganic nitrogen. Vasilakos et al., (2018) suggested that aerosol acidity is critical in the chemical transport model for the simulation response of $PM_{2.5}$ components to the change of precursor emissions. However, the studies on aerosol acidity have increased only recently, resulting in some unsolved problems (Pye et al., 2020). The current understandings and major challenges of aerosol acidity will be introduced in the following section.

1.3 Overview of previous studies on aerosol acidity

1.3.1 Earlier studies of aerosol acidity based on the proxy methods

In the earlier studies, researchers began to focus on aerosol acidity because of the potential adverse health effect and the acid deposition associated with aerosol acidity (Tanner et al., 1981). Because the collection and analytical methods of aerosol particles (e.g. filter collection and ion chromatograph analysis) and the measurement method of solution pH by pH probe (e.g. EPA Method IO-4.1) are widely used in atmospheric science, coupled with lack of direct measurement method for aerosol acidity, the aqueous extracts pH of aerosol samples is converted into the H^+ concentration per unit volume of air to be used as a proxy for aerosol acidity (e.g., Koutrakis et al., 1988; Sakamoto et al., 1994; Liu et al., 1996). However, the aqueous extracts pH cannot replace aerosol pH due to the different ionic strengths in aqueous extracts and aerosol liquid water. Thus, to distinguish them, the H^+ concentration calculated from the aqueous extracts pH is referred to as strong acidity ($[H^+]_{strong}$) referenced to the definition in the measurement method of solution pH (e.g., Pathak et al., 2004; Yao et al., 2006; Behera et al., 2015). When the data of the aqueous extracts pH is absence, the relationships between the water-soluble cations and anions are used to indicate the degree of acidity of aerosol particles (e.g., Yao et al., 2006; Zhou et al., 2018), which is under the assumption that H^+ exists in aerosol particles to balance the excess of anions.

Table 1 summarized the most commonly used proxy methods, such as strong acidity ($[H^+]_{strong}$), ion balance ($\Sigma cation - \Sigma anion$), and cation/anion equivalent ratio based on the concentrations of ionic species. Because the proxy methods are based on ionic analysis, the results are convenient to obtain in laboratory. Thus, it is still widely used in laboratory chamber studies (Surratt et al., 2007, 2010; Lewandowski et al., 2015).

However, the proxy methods do not consider gaseous components such as ammonia, which have a strong influence on the aerosol pH. Without the constraint of the gas phase, the proxy methods possess significant uncertainty (Guo et al., 2017b). Moreover, because the measurement conditions of proxy methods are quite different considering the ionic strength of aerosol particles, and ionic concentration measurements made in different laboratories do not agree well (Xu et al., 2020), these results do not necessarily reflect the real values of atmospheric aerosol pH. Additionally, the concentration of H^+ measured for

the aqueous extracts is not a conservative value (the non-conservative nature, Saxena et al., 1993). It does not scale in proportion to the level of dilution produced by buffering effects and the partial dissociation of weak acids (Hennigan et al., 2015). As a result, the proxy method results cannot completely replace aerosol acidity. However, many conclusions of aerosol acidity were obtained by using proxy method in earlier studies. But they are not worthless, only that the relationship between proxy method results and aerosol acidity should be revealed.

Table 1. Summary of the proxy methods. The unit for all chemical species is equivalent concentrations per unit volume of air (neq m^{-3}).

Proxy method	Formula
Measured acidity [a)]	Total concentration of H^+ in the aqueous extract of aerosol samples measured by the pH meter.
Ion balance [b)]	$[NH_4^+] + [Na^+] + [K^+] + [Ca^{2+}] + [Mg^{2+}] - ([SO_4^{2-}] + [HSO_4^-] + [NO_3^-] + [Cl^-])$
Cation/anion ratio [c)]	$\frac{[NH_4^+] + [Na^+] + [K^+] + [Ca^{2+}] + [Mg^{2+}]}{[SO_4^{2-}] + [HSO_4^-] + [NO_3^-] + [Cl^-]}$
Degree of sulfate neutralization [d)]	$\frac{[NH_4^+] - [NO_3^-]}{[SO_4^{2-}] + [HSO_4^-]}$
Degree of neutralization [e)]	$\frac{[NH_4^+]}{[SO_4^{2-}] + [HSO_4^-] + [NO_3^-]}$
Gas ratio [f)]	$\frac{[NH_3] + [NH_4^+] - [SO_4^{2-}] - [HSO_4^-]}{[HNO_3] + [NO_3^-]}$

[a)] Liu et al., 1996. [b)] Ito et al., 1998. [c)] Quinn et al., 2006. [d)] Solomon et al., 2014.
[e)] Adams et al., 1999. [f)] Ansari and Pandis, 1998.

1.3.2 Recent studies of aerosol acidity based on the thermodynamic models

As mentioned previously, the liquid phase of aerosol particles is different from the aqueous extracts of aerosol samples due to their different ionic strength and the non-conservative nature of H^+ concentration. Namely, the proxy method based on the analysis of aqueous extracts is defective for the studies of aerosol acidity. Therefore, the thermodynamic models are used to simulate atmospheric aerosol behaviors under a

designated temperature and RH, thereby estimating aerosol acidity by using the model output results such as the mole fraction activity coefficients of H^+ and the liquid water content of particles. Such models include the Extended Aerosol Inorganics Model (E-AIM, Wexler and Clegg, 2002), ISORROPIA II (Fountoukis and Nenes, 2007), SCAPE2 (Meng et al., 1995), and EQUISOLV II (Jacobson, 1999). Among them, the E-AIM model is regarded as the benchmark thermodynamic model for inorganic aerosol system, because it is based on the measurement thermodynamic data of pure aqueous solutions and mixtures (Wexler and Clegg, 2002; Pye et al., 2020) and its calculation is only based on the thermodynamic interactions among the solute species (Zaveri et al., 2008; Hennigan et al., 2015). Several studies have demonstrated that E-AIM model is more accurate and suitable to estimate aerosol acidity (Yao et al., 2006; Seinfeld and Pandis, 2016). For these reasons, E-AIM model is one of most commonly used methods in aerosol acidity studies.

Based on various input parameters including meteorological data, the concentrations of ionic species of aerosol particles, and gaseous data of NH_3 and HNO_3, E-AIM model provide a rigorous estimation of aerosol acidity. Among these input parameters, the data of gaseous NH_3 is much crucial because it strongly relates to the phase partitioning of NH_3/NH_4^+. Without NH_3 data, the estimation of aerosol acidity is expected to be highly uncertain. Namely, in the absence of NH_3, more NH_4^+ will be partitioned into the gas phase to remain the gas-particle equilibrium of NH_3/NH_4^+, resulting in the underestimation of NH_4^+ in particle phase (Hennigan et al., 2015; Song et al., 2018). As the unique alkaline inorganic component in aerosol particles, the underestimation of NH_4^+ will lead to an inaccurate estimation of aerosol acidity. Therefore, NH_3 data should be input into model to avoid the inaccurate phase partitioning of NH_3/NH_4^+. However, the gaseous NH_3 data are scarce and often neglected in many previous studies (e.g., He et al., 2012; Vieira-Filho et al., 2016). Furthermore, the observation of gaseous NH_3 and its corresponding particulate NH_4^+ under the same accuracy is more scarce because of the volatilization of NH_4^+ and adhesive characteristics of NH_3 (Osada et al., 2011). The different measurement techniques for NH_3 and NH_4^+ are likely to cause the mismatch of NH_3 and NH_4^+ (von Bobrutzki et al., 2010; Bae et al., 2007), resulting in misestimation of phase partitioning of NH_3/NH_4^+ in the thermodynamic model. In addition to lack of NH_3 data, long-term records for aerosol acidity are also rare. Most of previous studies mainly focused on a special period in a single

year, especially the haze period studies (e.g., Behera et al., 2015; Tian et al., 2018; Shi et al., 2019). However, a long-term study of aerosol acidity is necessary because many crucial parameters in atmospheric science change over prolonged periods such as temperature. The long-term study of aerosol acidity can reliably figure out the dominant factors affecting aerosol acidity and its temporal trend. Thereby, some acidity-dependent processes in the atmosphere can be predicted (e.g., in case of α-pinene formation, Surratt et al., 2007) and the influence of aerosol acidity can be parameterized in the risk assessment of ecosystem health and human health (e.g., in case of health risk, Behera et al., 2015). However, to date, only one previous study reported a long-term investigation of aerosol pH based on a comprehensive data by using E-AIM model (Tao and Murphy, 2020). Considering the lack of the long-term investigation based on the high-quality data set including NH_3, the studies of aerosol acidity needs to be continued.

On the other hand, to reduce the interference of sudden haze events in the long-term investigation of aerosol acidity, a less-polluted region should be considered as the study area. Moreover, with controlling of global air pollution, clean air worldwide could be achieved under policy interventions in the future (Amann et al., 2020). The study in a less-polluted region can provide a forecast of aerosol acidity for the areas where air pollution is decreasing year by year. Nagoya is exactly such region. Although Nagoya is a major urban city in Japan, concentrations of air pollution are not so high, as indicated by the annual mean value of $PM_{2.5}$ concentration (mass concentration of aerosol particles having aerodynamic diameter less than 2.5 μm) of about 12 μg m^{-3} in recent years, which is below the WHO interim target 3 (15 μg m^{-3}; WHO, 2017). Target 3 is the ultimate aim of the improvement in air quality that will be finally achieved in many countries (Rafaj et al., 2018).

Based the long-term data of Nagoya, including NH_3 and its corresponding particulate NH_4^+, the other species concentrations of aerosol particles, and meteorological data, the variation characteristics of aerosol acidity and its driving factors will be rigorously investigated by using E-AIM model. The results can supplement the long-term variations of aerosol acidity, reveal the dominant factors affecting aerosol acidity, and provide a forecast of aerosol acidity for the currently polluted but improving areas.

1.3.3 Importance of development for methods measuring aerosol acidity

Although the E-AIM model simulates aerosol inorganic behaviors accurately, it has a few weaknesses. The E-AIM model provide several output results, such as the ionic activity coefficients, the mole concentrations, the mole fractions and the molality concentrations. Based on different definitions or assumptions, aerosol acidity can be calculated by using some of these output results (Jia et al., 2018b; Pye et al., 2020). For example, the International Union of Pure and Applied Chemistry (IUPAC) defines pH as the negative logarithm of the product of H^+ molality concentration and its activity coefficient (IUPAC, 1997). While, Wexler and Clegg (2002) recommended that pH is equal to the negative logarithm of H^+ mole fraction multiplied by its activity coefficient. To date, there is no final conclusion for the most suitable equation in the estimation of aerosol acidity. Although Pye et al. (2020) gave the derivations of conversions between the different equations to help the intercomparison of the reports, this problem still prevents the proper understanding of atmospheric aerosol acidity. Therefore, a reliable measurement method for aerosol acidity that relates thermodynamic estimations with realistic atmospheric aerosol data should be developed.

However, because of low water content and high ionic strength of aerosol particles, the measurement method of aerosol acidity remains challenging. Recently, three semi-direct measurement methods for aerosol acidity were reported. One method uses colorimetry coupled with a reflectance UV–visible spectrometer to measure the absorbance change of a dyed indicator filter before and after aerosol sampling (Li and Jang, 2012; Jang et al., 2020). In this method, the H^+ concentration of an aerosol sample is calculated using the observed absorbance change. A second method uses Raman microspectroscopy to measure the concentration of an acid and its conjugate base (e.g., HSO_4^-/SO_4^{2-}, HNO_3/NO_3^-, etc.), the results of which are combined with extended Debye–Hückel activity calculations to determine the pH of aerosol particles (Rindelaub et al., 2016; Craig et al., 2017). A third method utilizes pH testing papers to measure aerosol acidity (Craig et al., 2018). In this method, aerosol samples are collected on the pH testing paper using a multiple-stage impactor. The pH of the aerosol sample is then observed from the resulting color of the pH testing paper. Although their tests were limited, Craig et al. (2018) demonstrated the potential of pH testing paper for measuring aerosol acidity. However, it

is widely recognized that pH testing papers are generally used to measure the pH of dilute solutions, while the liquid phase of aerosol particles is extremely high ionic strength because of the low water content. For example, the ionic strength of urban aerosol particles ranges from 7 to 45 M (Herrmann et al., 2015); therefore, the liquid phase of these particles cannot be considered as an ideal solution. Without the examination of the color response of pH testing papers in the presence of high ionic strength, the application of pH testing paper to aerosol particles is limited. Therefore, a newly reliable measurement method is required.

1.4 Research objectives

In view of the importance of aerosol acidity in atmospheric science and the various limitations of exiting studies, a comprehensive investigation of aerosol acidity is required. In this thesis, I have reviewed the current understandings and issues of aerosol acidity in Chapter1 to elucidate the motivation and purpose of this study. In Chapter 2, aerosol acidity is rigorously estimated by using the E-AIM model based on the 2-years data obtained in Nagoya, including continuous observation data of NH_3 and its corresponding particulate NH_4^+, the other ionic species concentrations of aerosol particles, and meteorological data. The model estimation results can elucidate the long-term variation characteristics of aerosol acidity and identify its dominant driving factor(s). Then, in order to relate the estimation results of Chapter 2 to the acidity of realistic atmospheric aerosol particles, a direct measurement method of aerosol acidity is developed by using pH testing paper and hygroscopic equilibrium under high relative humidity, and present in Chapter 3. The comparison between the estimation results based on E-AIM model and the detected results used by the newly-developed pH testing paper method is presented and discussed in Chapter 4, thereby drawing the conclusions about the variation characteristics and driving factors of aerosol acidity. Finally, the conclusions of this thesis are described in Chapter 5.

Chapter 2: Seasonal variation and driving factors of aerosol acidity analyzed by the E-AIM model based on the two-years data of Nagoya

Many previous studies attempt to characterize aerosol acidity, but it is still challenging to obtain the long-term variation characteristics of aerosol acidity and reliably identify its driving factors because of various limitations, such as the short time span of sample data (e.g., Zhou et al., 2018) and the lack of NH_3 data (e.g., Vieira-Filho et al., 2016). More detailed investigations of aerosol acidity are needed to improve the understanding of acidity-dependent chemical processes in the atmosphere (e.g., Surratt et al., 2010) and the assessment of ecosystem health and human health (e.g., Nenes et al., 2021; Raizenne et al., 1996). As far as the existing studies, the long-term continuous observation data for the estimation of aerosol acidity are still scarce, especially the gaseous NH_3 data and its corresponding particle NH_4^+ data. Due to the importance of NH_3/NH_4^+ gas-particle partitioning, their data should input into the model together to avoid the misestimation (Hennigan et al., 2015; Song et al., 2018). In this study, the continuous observations of gaseous NH_3 and its corresponding particle NH_4^+, gaseous HNO_3, the major ionic concentrations, temperature, and relative humidity were conducted in Nagoya from January 2017 through December 2018. Based on these high-quality continuous data, the E-AIM model was employed to estimate aerosol acidity and conduct several sensitivity tests for identifying its driving factors. Moreover, the aerosol data were obtained from less-polluted metropolitan area, the results are expected to be a representative for other less-polluted areas and a forecast for the worst air pollution areas.

2.1 Data sources and analysis method

2.1.1 Study area, sampling collection and chemical analysis

Nagoya, located in the central area of Honshu Island of Japan, near the coastline of the Pacific Ocean (Fig. 3), is the fourth largest metropolitan urban area (metropolitan Tokyo, Yokohama, Osaka, and Nagoya in order of population) in Japan. The Nagoya city residents of about 2.3 million live in an area of 326 km^2. Its busy port and Chukyo industrial areas

are located in the south, which serves as a major industrial hub in Japan. Major sources of local air pollution are associated with various forms of traffic (motor vehicles and ships), steel, machine and chemical industries, and agricultural activities in surrounding areas. Nonetheless, the air pollution level in Nagoya is low. The annual mean $PM_{2.5}$ concentration has remained about 12 μg m^{-3} in recent years (Nagoya City, 2019, http://www.city.nagoya.jp/kankyo/page/0000117927.html). The weather in Nagoya is mild (annual mean ambient temperature is 15.8°C), with adequate rainfall (annual mean rain amount is about 1500 mm), and four seasons that are governed mainly by warm, humid summer monsoon winds from the south with several typhoon arrivals and cold, dry winter monsoon winds from the northwest.

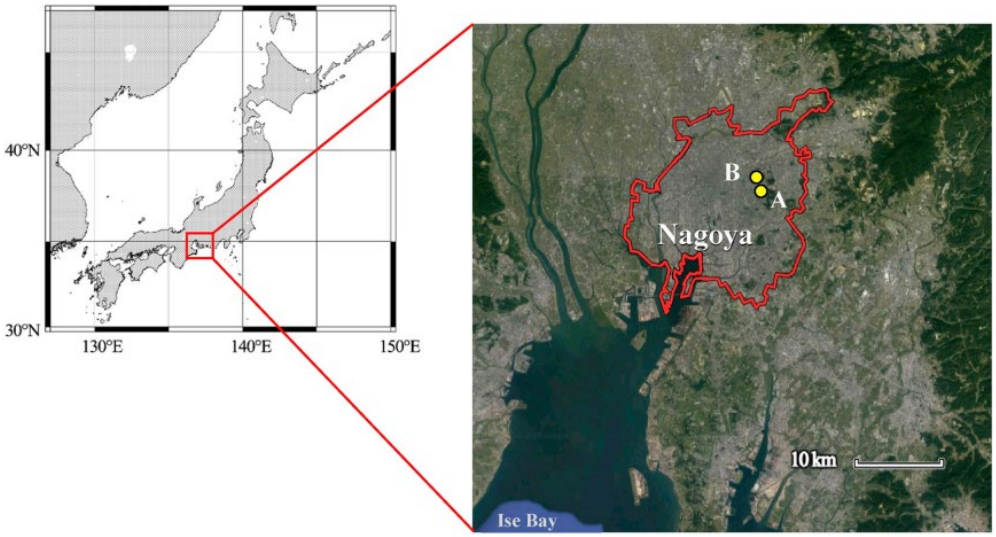

Figure 3. Left: location of Nagoya, Japan. **Right:** red line represents the city limits; A, Nagoya University observation site; B, Nagoya local meteorological observatory.

Atmospheric observations were conducted on the roof atop the seven-story Environmental Studies Hall (51 m above sea level; 35.16°N, 136.97°E) of Nagoya University (Fig. 3, A) from January 2017 through December 2018. A denuder and multistage filter system (DF system, Fig. 4) was used for gaseous nitric acid (HNO_3) and ionic constituents of size-segregated aerosols. The temporal resolution was typically 2–3 days and occasionally 8 hr to 1 day under high aerosol concentrations. After removing coarse particles using a Nuclepore membrane filter (8 μm pore size, 47 mm diameter;

Nomura Micro Science Co., Ltd.), HNO_3 was collected using an annular denuder (2000−30x242−3CSS; URG Corp.), which was coated inside with NaCl (Perrino et al., 1990). Fine aerosol particles were collected using a PTFE filter (pore size 1 μm; Advantec, Tokyo), and a nylon filter (Pall Corp.) to capture HNO_3 volatized from the PTFE filter (Appel et al., 1981; Vecchi et al., 2009). Ambient air was drawn into the DF system at a flow rate of 16.7 L min^{-1} (25°C, 1 atm). Under these conditions, the aerodynamic diameter of 50% cutoff for the nuclepore filter was about 1.9 μm (John et al., 1983). The filter samples (Nuclepore, PTFE and Nylon) were placed in air-tight polypropylene tubes and were stored in a refrigerator until extraction using 13 ml of pure water overnight. The extracts were analyzed for major ionic constituents (Cl^-, NO_3^-, SO_4^{2-}, $C_2O_4^{2-}$, Na^+, $NH_4^+{}_{(FP)}$, K^+, Mg^{2+}, Ca^{2+}) with an ion chromatograph (IC, LC-10A modified; Shimadzu Corp.). For this study, NO_3^- concentrations in fine particles were reported as the sum of data obtained from PTFE and nylon filters. For the extracts, pH was also measured using a pH meter (F-72; Horiba Ltd.) with a glass electrode (8103BNUWP ROSS Ultra; Orion Research Inc.). The H^+ concentration in the atmospheric aerosol extracts (strong acidity, $[H^+]_{strong}$) was calculated by subtracting the laboratory background value (3 μmol L^{-1}, approximated as the H^+ concentration in ultrapure water equilibrated with the laboratory CO_2 concentration of 700 ppm), and then dividing by the volume of air collected. For the annular denuder samples, 10 ml of pure water was added to extract NO_3^-. Then the extracts were measured using ion chromatography.

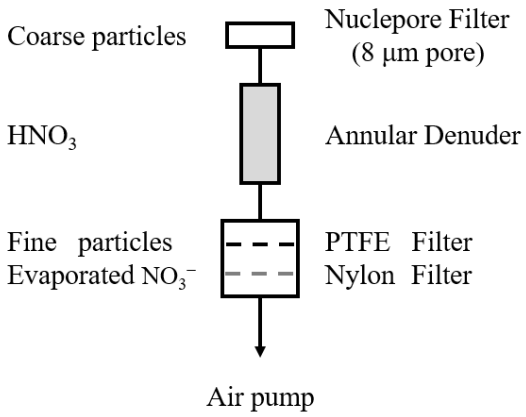

Figure 4. Configuration of the denuder and multistage filter system.

The concentrations of $NH_{3(g)}$ and $NH_4^+{}_{(P)}$ in fine particles were measured using a semi-continuous microflow (MF) analytical system (MF-NH3A; Kimoto Electric Co., Ltd.; Osada et al., 2011). Two identical sampling lines were used to differentiate total ammonium ($NH_{3(g)}$ and $NH_4^+{}_{(P)}$) and $NH_4^+{}_{(P)}$ after removal by a H_3PO_4-coated denuder. After passing an impactor (cut-off diameter of about 2 μm) and a glass tube (one coated; the other uncoated), pure water droplets were added to the sample air at 100 μl min^{-1}. The equilibrated sample water was analyzed respectively using a microflow fluorescence analyzer to quantify NH_4^+ in the lines of $NH_4^+{}_{(P)}$ and total ammonium. The concentration of $NH_{3(g)}$ was calculated using their difference. The sample air flow rate of the MF system was 1 L min^{-1}. The temporal resolution was 30 min for one pair of $NH_4^+{}_{(P)}$ and total ammonium measurements. Details of the MF system and atmospheric applications are presented elsewhere (Osada et al., 2011, 2019).

Hourly meteorological data (ambient temperature and relative humidity etc.) were obtained in Nagoya Local Meteorological Observatory (Fig. 3, B; data available from the official website https://www.jma.go.jp/jma/index.html). Data of the MF system ($NH_{3(g)}$ and $NH_4^+{}_{(P)}$) and meteorological parameters were averaged to fit the sampling time interval of the DF system.

2.1.2 Thermodynamic model

The E-AIM model, a semi-empirical model, runs in a stable state condition. Based on the minimization method of Gibbs free energy with respect to the composition and phase state of the particle, the model can calculate the phase behavior and gas-particle equilibrium in aerosol (Wexler and Clegg, 2002; Friese and Ebel, 2010). Depending on the input data, the E-AIM model can solve two types of problems, so-called forward and reverse modes (Fig. 5). For the forward mode, input data include ambient temperature (T), relative humidity (RH), and the total concentrations of gaseous and particle phases for NH_4^+ and NO_3^- with some other major ionic species depending on the versions of the E-AIM. It runs in a closed system in which the masses of chemical species are conserved. For reverse mode, input data include T, RH, and the concentration of chemical species in particle phase only. It assumes an open system so that the gas-phase partial pressures must be maintained at a constant value, presumably by continuous infusion of new air. As a

result, the mass balance is not satisfied because of the continuous addition of substances. The output of both modes is the concentration and various parameters of each of the species in gas, liquid, and solid phases. Compared to the forward mode, the reverse mode is more sensitive to the ion-balance of ionic species, which will cause large uncertainty of aerosol acidity estimation from the measurement error (Hennigan et al., 2015; Song et al., 2018).

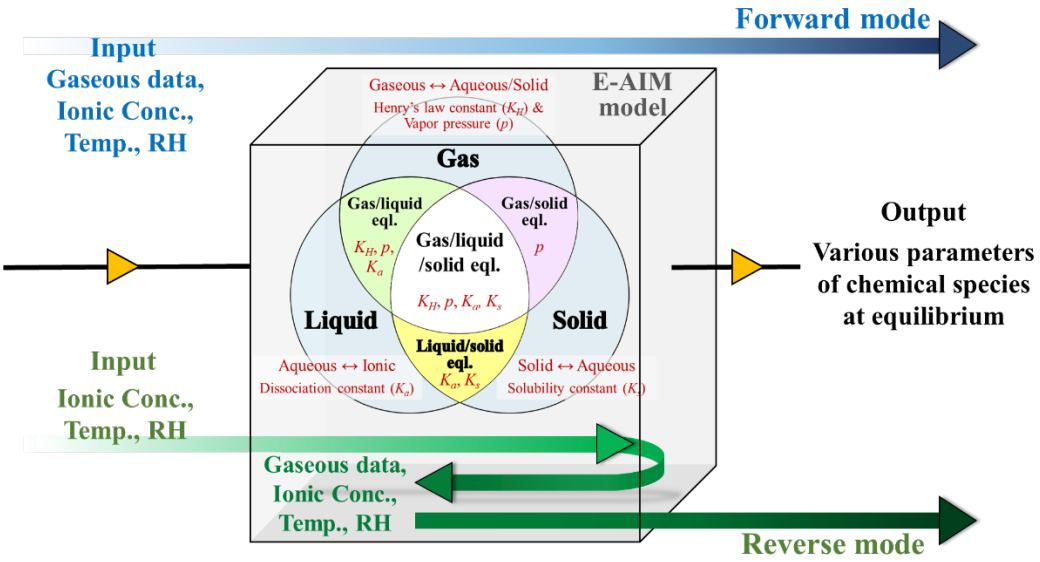

Figure 5. Schematic of the two modes of E-AIM model, including forward mode (blue arrow) and reverse mode (green arrow). The input data for forward mode include ambient temperature (T), relative humidity (RH), gaseous and ionic concentrations. While for revise mode, the input data are T, RH, and ionic concentrations. The output items of the two modes are the same, which are various parameters of chemical species at the equilibrium state.

The model simulates the behaviors of aerosol particles which place in the atmosphere, thus, "in situ" is used to highlight the place of simulated aerosol particles. In this study, that is in situ acidity and in situ pH, which were estimated using both modes of E-AIM model. The notation of pH_{IS} was used for the values based on both modes, and the notations of pH_{ISF} and pH_{ISR} were used for forward mode and reverse mode, respectively.

The E-AIM model has four versions (http://www.aim.env.uea.ac.uk/aim/aim.php). The AIM-IV was developed recently by Friese and Ebel (2010) for a

H^+–NH_4^+–Na^+–SO_4^{2-}–NO_3^-–Cl^-–H_2O mixture system under variable temperatures ranging from 263.15 K to 330 K and relative humidity higher than 60% (http://www.aim.env.uea.ac.uk/aim/model4/model4a.php). It can be regarded as a more authentic mode because AIM-IV covers more components such as sea salt particles: a key species at the coastal area. Typhoons (tropical cyclone) sometimes strike Japan. Therefore, atmospheric conditions are affected strongly by sea salt particles, especially in summer and autumn. The average relative humidity in Nagoya was 66%. Considering the sea salt effect, higher relative humidity, and availability of data on precursor gases, the forward mode of the AIM-IV was selected to estimate the particle acidity. There are 165 data used to calculate various parameters after screening average RH > 60% in the total air sample number of 286.

The E-AIM model outputs various parameters of aerosol particles. The in situ pH is calculated by using these parameters based on the formula of pH definitions. The original pH definition is the negative logarithm of H^+ activity in the liquid water (Stumm and Morgan, 1996). According to the practical operability of obtaining data, the formula can be transformed into several equations. The differences among these equations were described by Jia et al. (2018b), and also discussed further in Section 4.1 in this study. Leaving aside the difference of pH definition formulas, in this section, the following equation was used to calculate pH_{IS}, as described in the E-AIM model Tutorial: the activity of H^+ is equal to its mole fraction multiplied by its activity coefficient (http://www.aim.env.uea.ac.uk/aim/tutorial/lesson1a.htm).

$$\mathrm{pH}_f = -\log_{10}(a_{fH}) = -\log_{10}(f_H x_H), \quad (1)$$

where a_{fH} and f_H denote the mole-fraction-based activity and the activity coefficient of H^+, respectively. The x_H represents the mole fraction of H^+ in particles calculated as $x_H = \frac{n_H}{\sum_j n_j}$, where n_H is the moles of H^+, and $\sum_j n_j$ is the summation of all solution species j, including water.

2.2 Results and discussion

2.2.1 Ionic composition and measured acidity

Figure 6 presents the ionic concentrations measured by IC and H^+ calculated from pH measurements of solution extracted from aerosol samples (n=286). Filled circles (n=165) show samples for RH higher than 60%, on average, during sample collection. Samples with higher RH were obtained in all seasons. However, it was infrequent in spring. Concentrations of NH_4^+, SO_4^{2-}, and NO_3^- were much higher than those of other ions, with respective averages of 60.4 neq m^{-3}, 54.4 neq m^{-3}, and 17.6 neq m^{-3}. Both NH_4^+ and SO_4^{2-} concentrations showed a tendency to be high in summer and low in winter. As opposed to them, NO_3^- concentrations were high in winter and low in summer, presumably because of the dissociation of ammonium nitrate at higher temperatures. The average concentrations of Na^+ and Cl^- were, respectively, 3.8 neq m^{-3} and 2.8 neq m^{-3}. Sea salts include both ions but the Na^+ concentration is often used as an indicator of sea salts because Cl^- can be modified and can escape from particles as HCl (Vogt et al., 1996). In Nagoya, Na^+ concentrations were sporadically high in summer and autumn associated with arrival of typhoons with strong winds from the south. For example, high Na^+ concentrations were observed in early July and early September, 2018. Unlike Na^+, Cl^- showed lower concentrations in summer. Reports of earlier studies have described that Cl^- from sea salts tends to evaporate as HCl in summer after reacting with acidic substances (Kawakami et al., 2008; Xiao et al., 2018), which can affect aerosol acidity directly. The concentrations of K^+, Mg^{2+}, and Ca^{2+} were very low relative to the others. The concentrations of $[H^+]_{strong}$ were 0.4–27.5 neq m^{-3}, with the average of 5.4 neq m^{-3}, and were low in winter and high in other seasons with large variation.

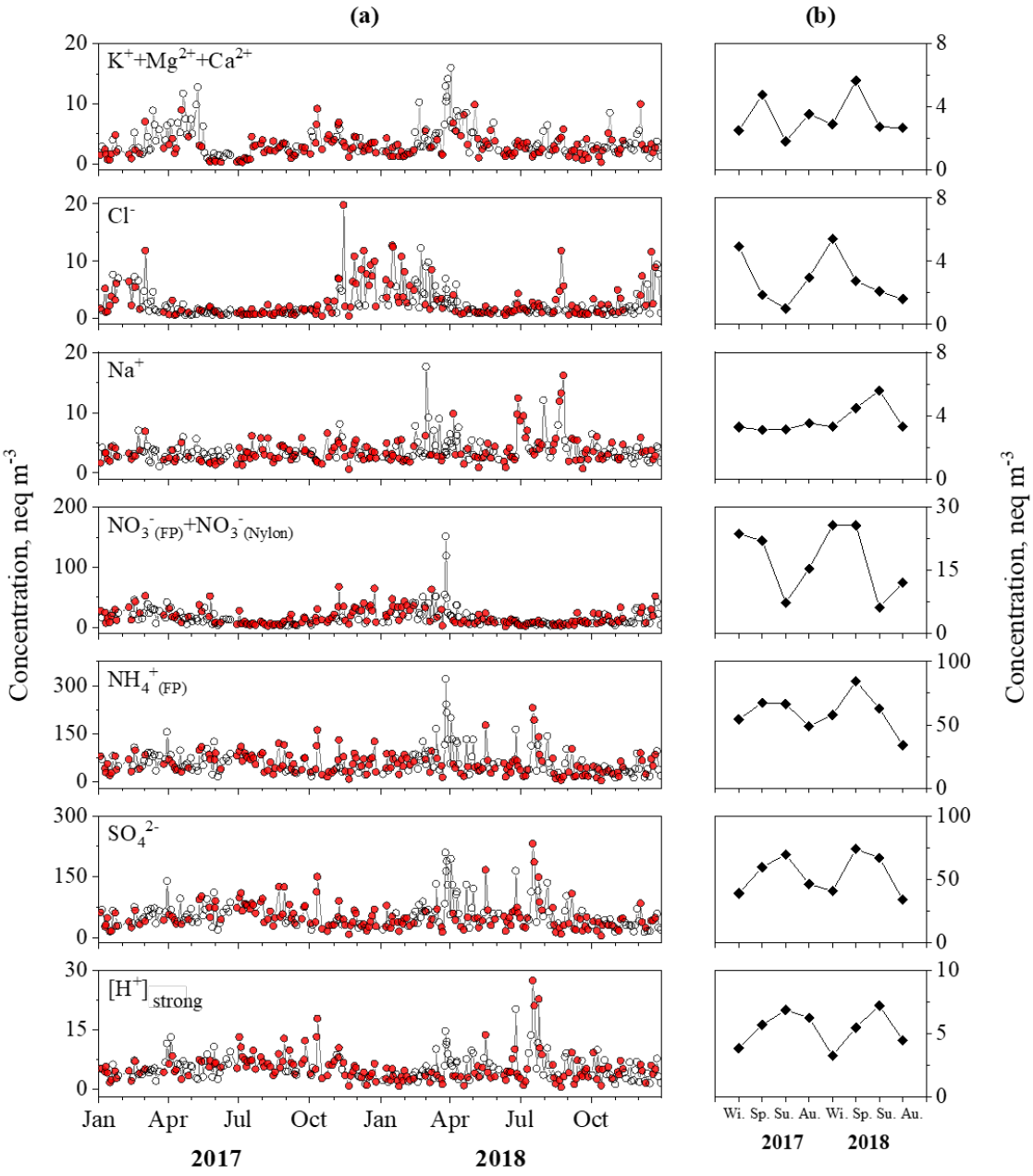

Figure 6. Left column: time series of ionic concentrations and measured acidity $[H^+]_{stong}$ of water extracts for fine particle samples (n=286). Filled circles (n=165) show data for samples with RH higher than 60% on average, subsequently used to estimate pH_{IS} using the E-AIM IV model. **Right column:** seasonal averages of ionic concentrations and $[H^+]_{strong}$. The ranges of respective seasons were winter – December, January, and February; spring – March, April, and May; summer – June, July, and August; autumn – September, October, and November.

Figure 7 shows the seasonal average of relative abundance (color bars) of ionic concentrations to the total amount in equivalent units and the seasonal average of $[H^+]_{strong}$ (black line): spring – March, April, and May; summer – June, July, and August; autumn – September, October, and November; winter – December, January, and February. The highest and nearly constant (38.8–44.6%) contributions to the total ionic constituents were found for NH_4^+. Contributions of SO_4^{2-} varied: they were higher in summer and lower in winter, in contrast to the trend shown for NO_3^-. The seasonal variation of $[H^+]_{strong}$ resembles that of the SO_4^{2-} contribution. Compared to the contributions of NH_4^+, SO_4^{2-}, and NO_3^- (together accounting for 91.3–96.0% of total ions), the contributions of other water-soluble ions (Cl^-, Na^+, K^+, Ca^{2+}, and Mg^{2+}) were minor (4.0–8.7% in total ions).

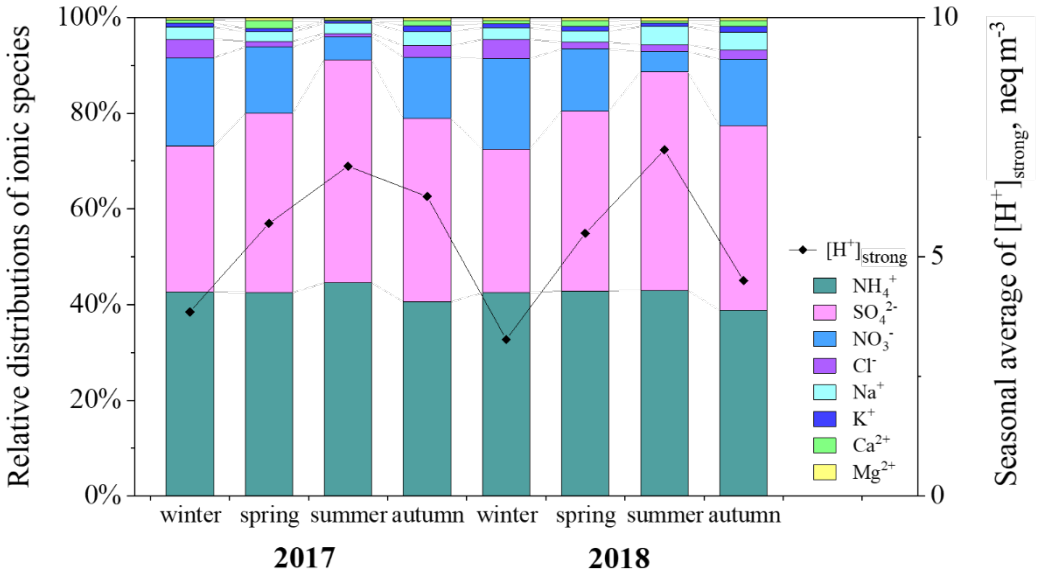

Figure 7. Relative distributions among water-soluble ionic species in fine particles based on equivalent concentrations. NO_3^- is the sum of data from PTFE and nylon filters; the other ionic concentrations were referred from data on PTFE filters. Black line with diamond symbols shows the seasonal average of measured acidity $[H^+]_{strong}$: winter – December, January, and February; spring – March, April, and May; summer – June, July, and August; autumn – September, October, and November.

Figure 8 presents scatter plots of the ionic balance between major anions and cations. As shown in Fig. 8a, the sum of major cations (NH_4^+(FP) and $[H^+]_{strong}$) correlates well (R^2=0.98) with the sum of major anions (SO_4^{2-} and NO_3^-). The slope (0.99) of the linear regression equation indicates that the major cations almost neutralized these anions. Among these parameters, the relation (Fig. 8b) between SO_4^{2-} and $[H^+]_{strong}$ also shows positive correlation (R^2=0.67, p<0.01), suggesting that the seasonal variation of $[H^+]_{strong}$ was affected by the SO_4^{2-} concentration.

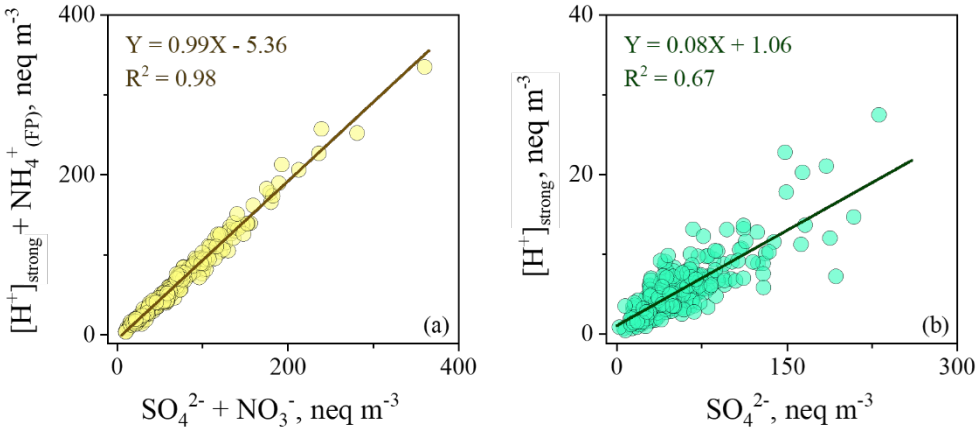

Figure 8. Relation between measured acidity $[H^+]_{strong}$ and the major ions: **(a)** correlation of (SO_4^{2-} + NO_3^-) with ($[H^+]_{strong}$ + NH_4^+(FP)) and **(b)** correlation of SO_4^{2-} with $[H^+]_{strong}$.

2.2.2 In situ pH of fine particles

Figure 9 presents values of in situ pH (pH_{ISF}, bottom) estimated using forward mode of the E-AIM IV model with various data used for estimation, and extreme values marked as filled circles in red. Gray thin lines in Fig. 9 show their seasonal averages as the same seasonal division in Fig. 7. The pH_{ISF} was 3.68–5.37 with the average of 4.44 ± 0.39, exhibiting a clear seasonal variation that is low in summer and high in winter. In 2017, the lowest value of pH_{ISF} (3.68) appeared for the sample taken during July 10–12. In this sample, NH_3 concentrations were much lower (112 nmol m^{-3}) than the summer average (236 nmol m^{-3}). The highest value of pH_{ISF} in 2017 (5.12) was obtained for the sample taken during January 13–16. In this sample, the SO_4^{2-} concentration was very low: 6.89

nmol m^{-3} compared to its winter average of 18.6 nmol m^{-3}. In 2018, the lowest value of pH_{ISF} (3.82) was also found in summer, with the sample taken during June 26–28. In this sample, the NH_4^+ concentration was lower (87.5 nmol m^{-3}) than its summer average (105 nmol m^{-3}).

The highest value (5.37, denoted as "#") of pH_{ISF} in the study period was found for the sample taken during August 22–24, 2018. During this period, Nagoya was buffeted by double typhoons (Soulik, August 15–25 and Cimaron, August 16–24), which moved from southwest to west of Nagoya. Because of the counterclockwise movement of winds around those typhoons, strong southerly winds brought sea salt particles from the Pacific Ocean to Nagoya area. Indeed, both Na^+ and Cl^- concentrations in the sample were much higher (13.2 nmol m^{-3} and 11.8 nmol m^{-3}, respectively) than their respective averages of 3.6 nmol m^{-3} and 3.0 nmol m^{-3}.

To deduce sea salt effects on in situ pH, I compared the results with those estimated using AIM-II (forward mode), which runs in a $H^+–NH_4^+–SO_4^{2-}–NO_3^-–H_2O$ system (Clegg et al., 1998) without Na^+ and Cl^-. In $H^+–NH_4^+–Na^+–SO_4^{2-}–NO_3^-–Cl^-–H_2O$ system (E-AIM IV), solid phase of sodium sulfate was formed with Na^+ and SO_4^{2-} because atmospheric RH (80%) was lower than the DRH (85%) of Na_2SO_4 (Tang and Munkelwitz, 1994), which is expected to reduce SO_4^{2-} in liquid phase. Cl^- can be evaporated by reaction with other inorganic acids (Kawakami et al., 2008; Xiao et al., 2018), which is expected to reduce the H^+ in liquid phase. Because of the two mechanisms, pH_{ISF} estimated from the AIM-II (3.78) was much lower than that of AIM-IV, suggesting significance of fresh sea salts for raising pH of particles. A similar result was reported for the existence of Na^+ and NH_4^+ to SO_4^{2-} ratio in a thermodynamic model (ISORROPIA II; Guo et al., 2018). Because of the large difference of pH obtained in this study together with others, sea salt particles should be included in pH_{IS} estimation for coastal areas, which are often affected by sea salt particles.

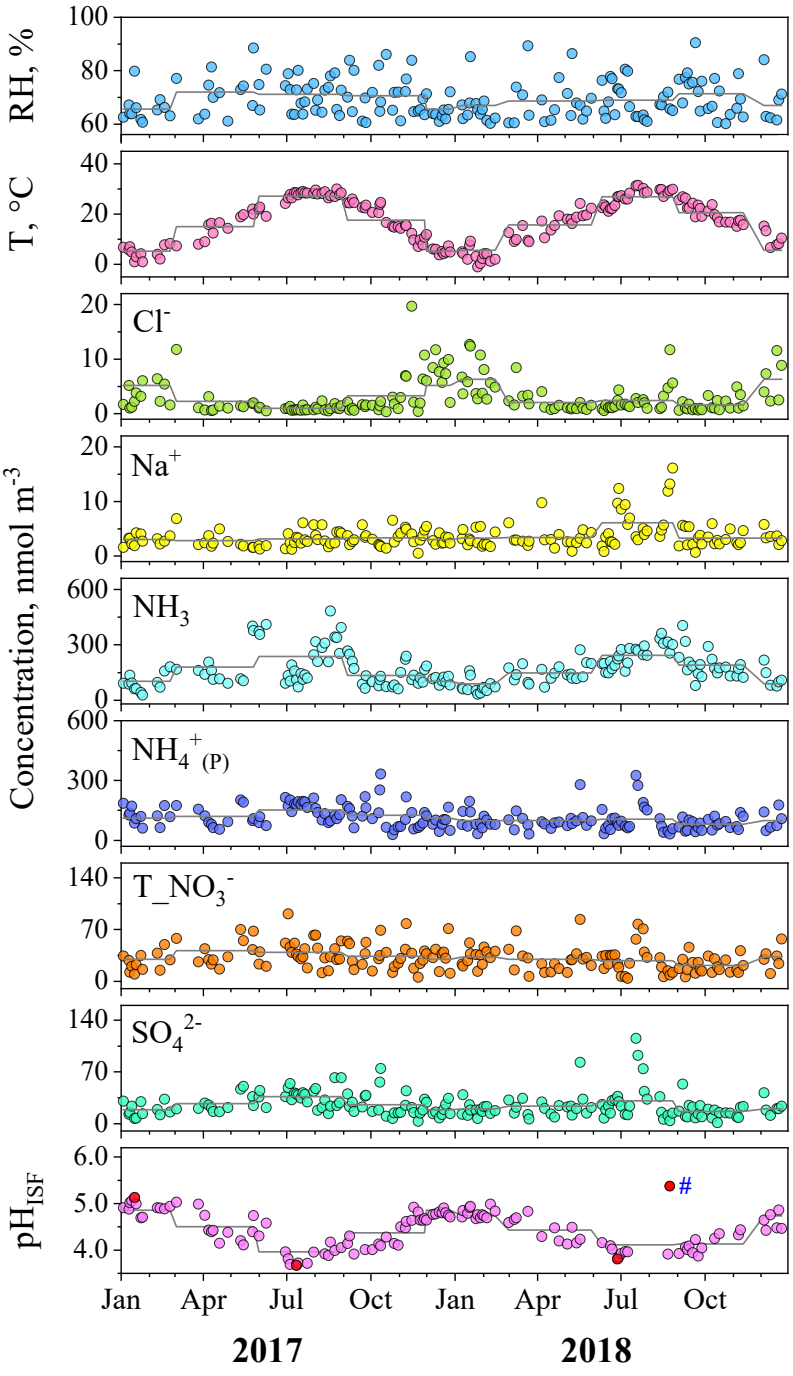

Figure 9. Time series of data used for estimating pH_{ISF}. Extreme values marked in red and the highest value marked with "#". T_NO_3^- represents the total nitrate (NO_3^- plus HNO_3). Gray thin lines show seasonal averages.

As presented in Fig. 9, air temperature in Nagoya also shows seasonal variation, which varies inversely with pH_{ISF}. Figure 10 shows the relation between ambient temperature and pH_{ISF}, excluding the highest value of pH_{ISF} (5.37, denoted as "#") taken during August 22–24. Strong correlation (R^2=0.83, p<0.01) was found for these, indicating that temperature is an important factor driving the seasonal variation of pH_{ISF}. The derivative of pH_{ISF} dependence on temperature is $\frac{d\,pH_{ISF}}{d\,T}$ = -0.04, which corresponds to increasing temperature by 2.5 °C decreases the pH unit by 0.1. Similar results (-0.05 per Kelvin) were observed in Canada (Tao and Murphy, 2019). The temperature effects on pH_{ISF} estimation of particles are discussed further in section 2.2.4.

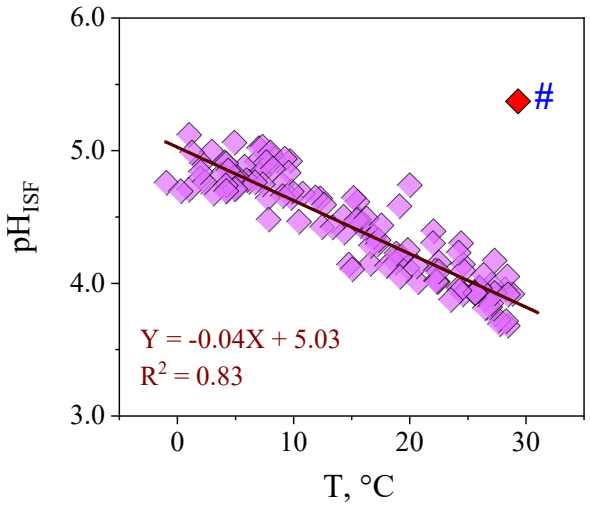

Figure 10. Relation between air temperature and pH_{ISF}. The regression line and the equation shown in the figure were calculated by excluding the highest value of pH_{ISF} (5.37, marked in red with "#").

It is particularly interesting that the seasonal variation of pH_{ISF} is similar to the seasonal tendency of $[H^+]_{strong}$, which is high in summer and low in winter. To examine the relation between pH_{IS} and $[H^+]_{strong}$ further, the $pH_{ISF\text{-}95\%}$ was estimated using the E-AIM IV forward model assuming a fixed RH of 95% for all samples (n=286). Estimation of $pH_{ISF\text{-}95\%}$ provides more data pairs for comparison between in situ pH of particles and pH of extracted samples. The results are presented in Fig. 11b ($pH_{ISF\text{-}95\%}$) and 11c ($[H^+]_{ISF\text{-}95\%}$). The seasonal variation of $pH_{ISF\text{-}95\%}$ was nearly parallel with that of pH_{ISF} (Fig. 11a, n=165):

it was shifted upward by 0.50 pH units, on average. Significant correlation (R^2=0.91, p<0.01) between $pH_{ISF\text{-}95\%}$ and pH_{ISF} is portrayed in Fig. 11e. The highest value of pH_{ISF} (5.37, denoted as "#") taken from August 22–24 is an outlier in Fig. 11e. Sea salt particles have strong hygroscopicity (Seinfeld and Pandis, 2016; Snider et al., 2006). Therefore, this sample containing higher Na^+ and Cl^- is presumably deviated from the relation obtained for other samples. Data of $[H^+]_{ISF\text{-}95\%}$ (Fig. 11c) were calculated as the number of moles of free H^+ in particles per unit volume of air assuming RH at 95%. The high RH (95%) can engender a high aerosol liquid water content (ALWC). Most of the components will dissolve in liquid phase. As a result, the liquid phase in the aerosol is close to the solution extracted from aerosol samples. As shown in Figs. 11c and 11d, $[H^+]_{ISF\text{-}95\%}$ and $[H^+]_{strong}$ exhibit closely similar temporal variations, implying that in situ acidity at high RH without a large contribution of nonvolatile cations is closely related to the measured acidity of the extracted solution. Their absolute values differ because of the activity coefficient dependence on ALWC. As described in section 2.2.1, a positive correlation between $[H^+]_{strong}$ and SO_4^{2-} in extracted solutions suggests that the seasonal variation of $[H^+]_{strong}$ was affected by SO_4^{2-}. Similarly, I tried to compare $[H^+]_{ISF\text{-}95\%}$ and SO_4^{2-}, as portrayed in Fig. 11f. Weak positive correlation (R^2=0.52, p<0.01) was found between them, suggesting that SO_4^{2-} partly affected $[H^+]_{ISF\text{-}95\%}$.

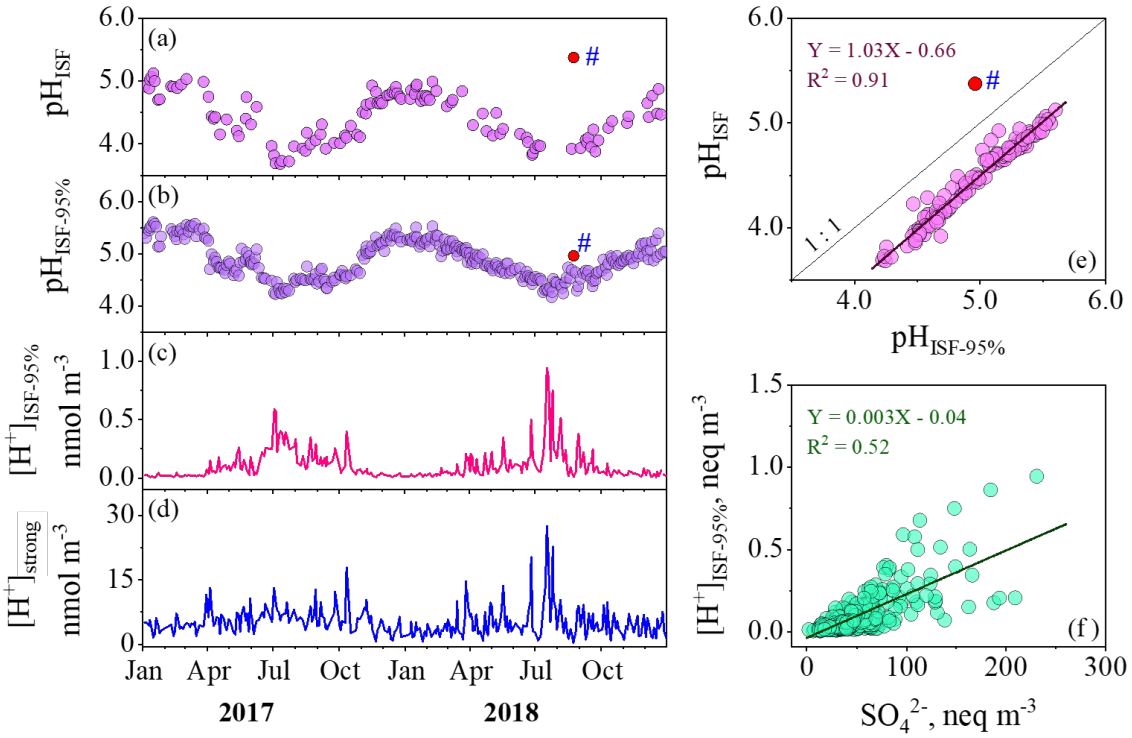

Figure 11. (a–d) Time series of pH_{ISF}, $pH_{ISF\text{-}95\%}$, $[H^+]_{ISF\text{-}95\%}$, and $[H^+]_{strong}$. $pH_{ISF\text{-}95\%}$ and $[H^+]_{ISF\text{-}95\%}$ are simulated results obtained using the E-AIM IV forward model assuming a fixed RH of 95% for all samples (n=286). **(e)** Relation between $pH_{ISF\text{-}95\%}$ and pH_{ISF}, the outlier marked in red with "#". **(f)** Relation between SO_4^{2-} concentration and $[H^+]_{ISF\text{-}95\%}$.

Although Nagoya is located near the ocean coast, strong contributions of fine sea salt particles and other nonvolatile cations are not so common. Generally, the concentrations of fine sea salt particles are not high in Nagoya. To avoid miscalculation of pH_{IS} in some particular period, fine sea salt particles should also be considered. However, for the seasonal variation of in situ acidity and pH_{IS}, the major factors are air temperature and SO_4^{2-} concentration. A similar conclusion was reported in Beijing that temperature and SO_4^{2-} were two of the driving factors affecting the seasonal variation of aerosol acidity (ISORROPIA II; Ding et al., 2019).

2.2.3 Comparison with other studies

Table 2 presents (1) the average concentrations of chemical compositions and values of pH_{IS} using forward and reverse modes for samples (n=165) with RH > 60% in this study and (2) data from earlier studies using E-AIM at other places. As presented in Table 2, the average value of pH_{IS} in Nagoya was the highest among reports used by the E-AIM model. Estimation using the reverse mode did not require gaseous data for NH_3 and HNO_3 for the input data. Therefore, most earlier studies have used reverse mode of various versions of the E-AIM. Only a few studies used forward mode of the E-AIM, such as those reported by Hennigan et al. (2015) and by Tao and Murphy (2019). Because of the different versions and modes used in those earlier studies, all the results are difficult to compare. Generally, as Table 2 shows, the concentrations of $PM_{2.5}$ and ionic constituents in Nagoya were much lower than those at other sites, especially for the major anions. The concentrations of SO_4^{2-} (25.2 nmol m^{-3}) and NO_3^- (16.4 nmol m^{-3}) in Nagoya were one-half to one-tenth of those in many Chinese cities: for example, concentrations of SO_4^{2-} in Chongqing (253 nmol m^{-3}, He et al., 2012) and NO_3^- in Beijing (160 nmol m^{-3}, Pathak et al., 2009) were about 10 times higher than those found in the present study. The values of pH_{IS} for Chinese cities in Table 2 were much lower than those in Nagoya. In Mexico and the Po Valley, the concentrations of major ions were approximately equal to those found in this study. The values of pH_{IS} were also close to those found for Nagoya. These comparisons imply that lower ionic concentrations in Nagoya might be one factor underlying its higher pH_{IS}. The effects of ionic concentrations on pH_{IS} estimation will be discussed in section 2.2.4 based on various sensitivity tests. In addition to differences in the concentrations of inorganic constituents, organic substances might also modify ALWC. Water-soluble organic substances in fine particles absorb water proportionally to their organic fraction (Dick et al., 2000). Guo et al. (2015) showed that increasing organics increased ALWC, producing lower acidity of particles. In this study, concentration of oxalate in Nagoya was 1.08 nmol m^{-3}. Oxalate is the representative organic acid of water-soluble organics. Comparing oxalate concentrations to those of other cities such as Chengdu, China (6.1−15.3 nmol m^{-3}, Cheng et al., 2015), organic effects on in situ pH are not expected to be large.

Table 2. Ionic concentrations (nmol m^{-3}), $PM_{2.5}$ (μg m^{-3}), trace gases (ppb), and pH_{IS} in Nagoya (n=165) from this and other studies

Location	Period	NH_4^+	SO_4^{2-}	NO_3^-	Na^+	Cl^-	NH_3	HNO_3	$PM_{2.5}$	Model[b]		pH_{IS}	Reference
Nagoya[a]	2017–2018	112±56.7	25.2±16.8	16.4±13.5	3.64±2.26	2.98±3.18	4.04±2.18	0.362±0.344	11.7±5.16	AIM-IV	R F	3.88±0.58 4.44±0.39	This study
Tanggu	2013	500	240	210	13.0	50.7			132	AIM-II	R	1.3	Zhou et al. (2018)
Bohai		444	260	135	21.7	25.4			142			1.2	
Mexico	2006	93.9	39.0	47.3	13.5	7.61	25.2	2.43		AIM-IV	R F	2.36 3.24	Hennigan et al. (2015)
Po Valley	2009	127	36.3	62.4					30.7	AIM-IV	R	3.15	Squizzato et al. (2013)
Beijing	2005–2006	378	150	134	17.4	36.6			93.5	AIM-II	R	−0.6–0.4	He et al. (2012)
Chongqing		422	253	80.6	26.1	39.4			130			0.5–1.4	
Toronto	2007–2016	56.5	17.6	26.1			3.16	0.72		AIM-II	F	2.62	Tao and Murphy (2019)
Simcoe		53.7	18.8	20.2			2.01	0.46				2.41	
Windsor		64.8	22.5	26.8			2.01	0.68				2.27	
Ottawa		35.1	12.4	14.1			1.97	0.41				2.54	
Montreal		32.7	11.7	14.0			2.13	0.44				2.35	
St. Anicet		36.2	12.2	13.7			2.08	0.32				2.51	
Chengdu[c]	2011	350–833	188–375	177–339	47.8–187	42.3–200				AIM-II	R	−2.3–2.1	Cheng et al. (2015)
Hong Kong	2008–2009	172	104	29.7	19.1	7.89				AIM-III	R	−0.03	Xue et al. (2011)
Beijing	2005	261	235	160	4.35	11.3			68.0	AIM-IV	R	−0.52	Pathak et al. (2009)
Shanghai		228	165	115	17.4	53.5			67.0			−0.77	
Lanzhou	2006	227	102	51.6	21.7	155			65.0			−0.38	
Guangzhou	2004	267	136	83.9	17.4	25.4			55.0			0.61	
Guangzhou	2013	282	118	44.5	6.96	9.86				AIM-III	F	1.5–3.4	Jia et al. (2018a)

[a] Results for Nagoya were averaged for the aerosol samples (< 1.9 μm, n=165) with RH > 60%.

[b] Letters "R" and "F" respectively denote reverse and forward modes.

[c] Particle size in Cheng's study was < 2.1 μm.

2.2.4 Factors affecting seasonal variation of in situ pH of fine particles

Based on results of analyses explained up to this point, the possible factors affecting pH_{IS} were air temperature and major ionic constituents (especially SO_4^{2-} concentration). To assess these factors, the pH_{IS} was tested under different conditions by changing factors one by one while fixing other factors. The initial condition was set as the average ionic concentrations of samples (n=165) with RH > 60%, including T_0 (17.4°C), RH_0 (0.70), as presented in Table 2. The initial pH_{IS} was also used from the average in Table 2.

To characterize the effects of temperature on pH_{IS} estimation, RH and the ionic concentrations were fixed. The temperature was changed by raising it by 5 °C, 10 °C, and 15 °C from T_0, and by lowering it by 5 °C and 10 °C. Figure 12a presents pH_{IS} estimated using both forward and reverse modes under different temperature conditions, and colored by the ALWC. In either mode, pH_{IS} decreases considerably with increasing temperature. The rate of decrease versus the temperature increase is almost identical in the two modes: increasing temperature by 2 °C can be expected to decrease the pH unit by 0.1 ($\frac{d\,pH_{IS}}{d\,T}$ = -0.05). It is slightly different from the result explained in section 2.2.2 (-0.04 per Kelvin in Nagoya), indicating that temperature is not the only factor affecting seasonal variation of pH_{IS} in Nagoya. Moreover, as the ALWC indicated by the color of the pH_{IS} in Fig. 12a, clear reduction of the ALWC can be found with increasing temperature. The reduced ALWC has a concentrating effect on the free H^+ in particles. It can enhance the ionic strength of free H^+, resulting in lower pH_{IS}. Therefore, the major pathway of temperature effects on pH_{IS} is the result of changing the ALWC with temperature. A similar result was described by Ding et al. (2019) using ISORROPIA II. However, correlation between temperature and pH_{IS} was not clear in some aerosol acidity studies (Pathak et al., 2009; He et al., 2012; Cheng et al., 2015; Zhou et al., 2018). The concentrations of the major ionic constituents in these studies were very high (Table 2). Therefore, the temperature effects on pH_{IS} with different concentrations of major ions were assessed.

Considering the high proportion of SO_4^{2-} in all anions as described in section 2.2.1, it is selected firstly to test the temperature effects on pH_{IS}. Relative humidity and other ionic concentrations were fixed. Then the SO_4^{2-} concentrations were multiplied from 1 to 10 times from the initial concentration of 25.2 nmol m^{-3}. Figure 12b shows pH_{ISF} estimated by the forward mode under different temperature conditions and SO_4^{2-} concentrations

represented by color. At higher SO_4^{2-} concentrations, pH_{ISF} increased slightly with the increase of temperature. However, below a certain value of SO_4^{2-} concentration, the temperature effects became strong, which demonstrated that pH_{ISF} decreased with increased temperature. The value obtained using this simple sensitivity analysis was 126 nmol m^{-3} lower than the SO_4^{2-} concentrations of most Chinese sites in Table 2. This finding is consistent with the fact that no correlation was reported based on results obtained for these sites. Therefore, the temperature effect on pH_{IS} estimation is limited by the concentration of chemical compositions. At low air pollution sites, temperature is the major factor affecting pH_{IS}, as reported for Canada by Tao and Murphy (2019).

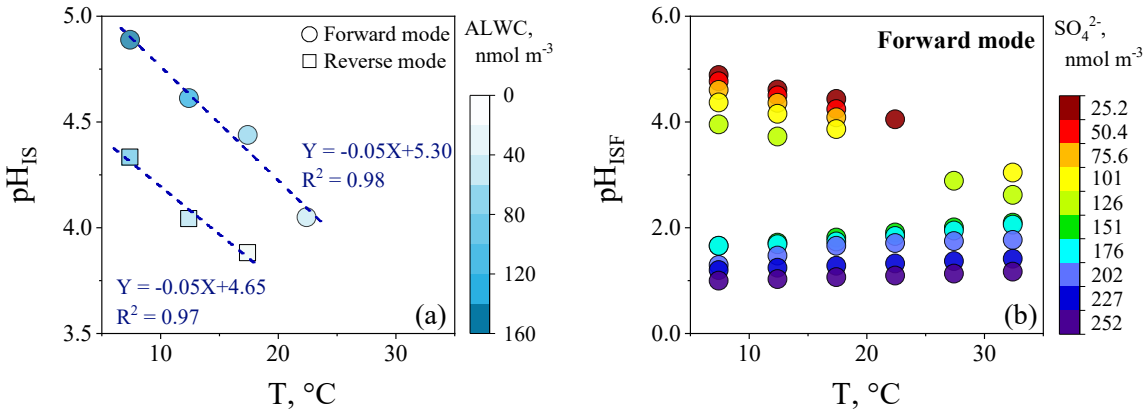

Figure 12. Effects of ambient air temperature on pH_{IS} estimation. **(a)** pH_{IS} estimated by both forward mode (circles) and reverse mode (squares) under different temperatures with the fixed RH and ionic concentrations at the initial values. pH_{IS} is colored by the aerosol liquid water content (ALWC). **(b)** pH_{IS} estimated using forward mode under different temperatures and SO_4^{2-} concentrations with fixed RH and other ionic concentrations at initial values.

As discussed in section 2.2.3, higher pH_{IS} in Nagoya than that found in many other earlier studies might result from lower ionic concentrations in fine particles. The effects of concentration levels and key species of ionic compositions on pH_{IS} were examined as the following: (1) the concentrations of all the chemical compositions (NH_4^+, SO_4^{2-}, NO_3^-, Na^+, Cl^-, NH_3, and HNO_3) were increased by 1.5–5 times; (2) in the forward mode, the concentration of total nitrate (T_NO_3^-, equaling to NO_3^- plus HNO_3) was increased by 1.5–

5 times. Similarly, in the reverse mode, only the NO_3^- concentration was increased by 1.5–5 times; (3) the SO_4^{2-} concentration was increased by a factor of 1.5–5; (4) the NH_4^+ concentration was reduced by 1.5–5 times. These sensitivity experiments were conducted using the average values of temperature and RH at the initial values.

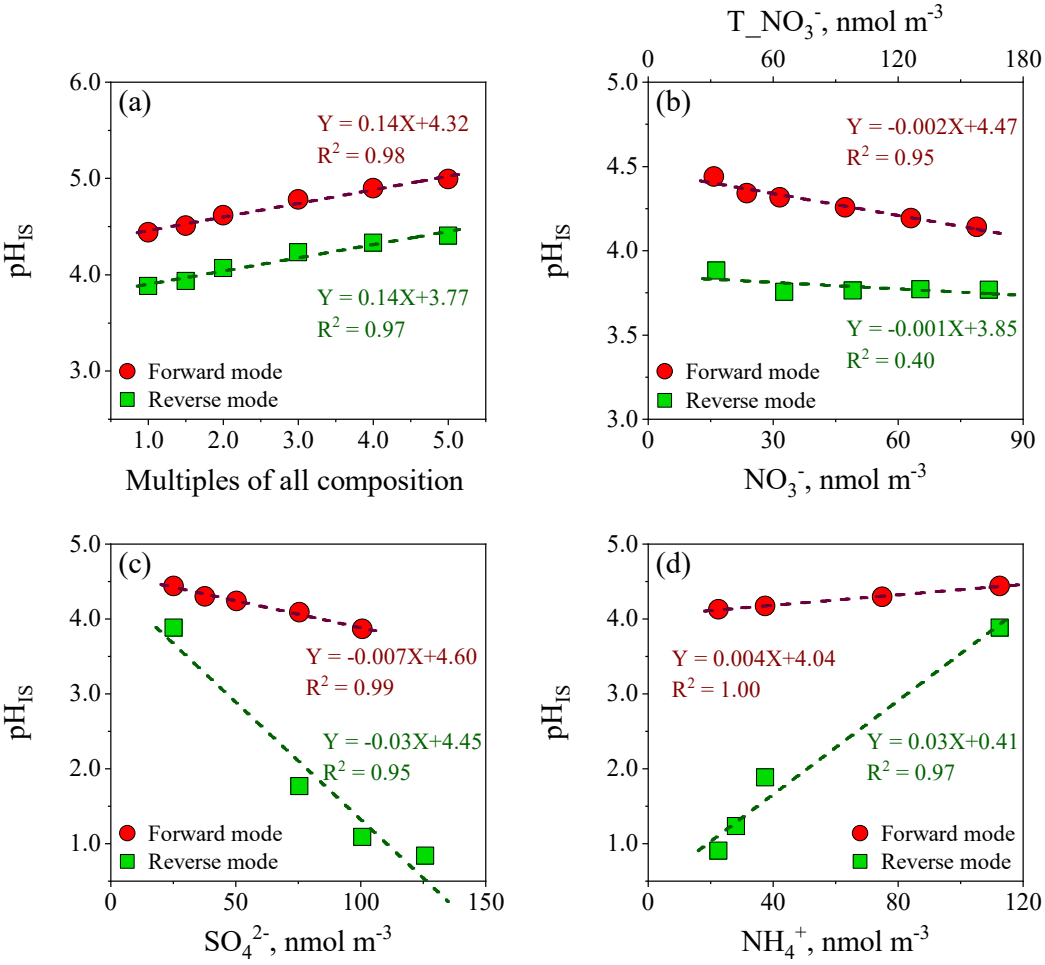

Figure 13. Effects of concentrations on pH_{IS} estimation. The pH_{IS} estimated by both forward and reverse modes under different ionic concentrations with fixed T and RH at the initial values: **(a)** all ionic concentrations were multiplied to 1.5–5 times; **(b)** T_NO_3^- was increased to 1.5–5 times in the forward mode, with the NO_3^- concentration increased in the reverse mode; **(c)** SO_4^{2-} concentration was increased to 1.5–5 times; **(d)** NH_4^+ concentration was reduced by 1.5–5 times.

Figure 13 presents results of the sensitivity experiments. When the concentrations of all ionic constituents were increased, the values of pH_{IS} increased concomitantly with increasing concentrations monotonically for both the forward and the reverse modes (Fig. 13a). In contrast, when the concentration of a single major ion was modified, the values of pH_{IS} changed variously among the relevant species (Fig. 13b for NO_3^- or T_NO_3^-; Fig. 13c for SO_4^{2-}; Fig. 13d for NH_4^+). Compared with NH_4^+ and SO_4^{2-}, changing NO_3^- (or T_NO_3^-) concentration had only a slight effect on pH_{IS} (Fig. 13b). The contributions of SO_4^{2-} and NH_4^+ on pH_{IS} were strong and showed similar behavior to that of the concentration change. Figure 13c shows that the values of pH_{IS} decreased concomitantly with increasing SO_4^{2-} concentration. In the forward mode, pH_{IS} declined slowly because of the buffering effects from NH_3 vapor–liquid equilibrium. In the reverse mode, the values of pH_{IS} were more sensitive to SO_4^{2-} concentrations. Then they declined sharply. For the contribution of NH_4^+ on pH_{IS}, the values of pH_{IS} decreased concomitantly with increasing NH_4^+ concentration. Considering that the initial concentration of NH_4^+ in Nagoya is lower than those reported from other studies (Table 2), the high pH_{IS} in Nagoya is not solely attributable to changes in NH_4^+ concentration, although tests proved that NH_4^+ has a slight effect on pH_{IS}. Because the concentrations of NO_3^- and SO_4^{2-} in this study are much lower than those of most other sites, and because the NO_3^- concentration has little effect on pH_{IS}, the major factor affecting pH_{IS} for Nagoya is the SO_4^{2-} concentration.

Results of sensitivity experiments presented above are consistent with the discussion in sections 2.2.2–2.2.3 indicating that the seasonal variation of pH_{IS} in Nagoya is strongly affected by ambient air temperature and the SO_4^{2-} concentration.

2.3 Chapter summary

In this chapter, a rigorous investigation of aerosol acidity was conducted by using E-AIM model based on a set of high-quality continuous data of NH_3 and its corresponding NH_4^+, HNO_3, ionic components of particles, temperature, and RH in Nagoya during 2017–2018. The major water-soluble ions in water extracts were NH_4^+, SO_4^{2-}, and NO_3^-. The strong acidity ($[H^+]_{strong}$) calculated from the pH measurements of extracted samples showed seasonal variation, high in summer and low in winter, which correlates with SO_4^{2-}

concentration (R^2=0.67), suggesting that the major factor driving its seasonal variation was the SO_4^{2-} concentration.

The in situ pH was estimated by the forward mode of the E-AIM IV model, showed that high in winter and low in summer. The seasonal variation of pH_{ISF} correlated well and significantly with air temperature (R^2=0.83, excluding the highest value), suggesting temperature as an important factor driving the seasonal variation of pH_{ISF}. The highest value of pH_{ISF} appeared on the sample taken during August 22–24, 2018, which contained high Na^+ and Cl^- concentrations influenced by oceanic air masses. Compared with other studies using the E-AIM models, pH_{IS} in Nagoya was higher than at other sites where major ionic concentrations were much higher than those in Nagoya.

To assess these factors affecting pH_{IS} suggested by initial analysis, various sensitivity tests were conducted using the E-AIM IV models by changing factors one by one while fixing the other factors. Sensitivity tests of temperature showed that pH_{IS} decreased concomitantly with increasing temperature. Based on analysis of the temperature effects with related parameters, temperature dependence of the ALWC was the main moderator of the temperature effect. Furthermore, sensitivity tests on the temperature combined with the SO_4^{2-} concentration indicated a critical threshold (ca. 126 nmol m^{-3}) of the SO_4^{2-} concentration on the effect: the temperature effect on pH_{IS} was only found below the threshold concentration. In addition, sensitivity tests of ionic species showed that changes in the SO_4^{2-} or NH_4^+ concentration exerted the strongest effect on pH_{IS}. Therefore, considering that the initial concentration of NH_4^+ in Nagoya was low, the major factor affecting pH_{IS} was the SO_4^{2-} concentration. With increasing SO_4^{2-} concentration, the pH_{IS} value declined slowly because of buffering effects from NH_3 vapor–liquid equilibrium in the forward mode. These results are consistent with those of the initial analysis based on observations indicating that the major factors affecting pH_{IS} of fine aerosols in Nagoya are air temperature and the SO_4^{2-} concentration in the particles.

Chapter 3: Development of a direct measurement method for aerosol acidity using pH testing paper and hygroscopic equilibrium under high relative humidity

Aerosol acidity is important to many atmospheric chemical processes (e.g., Han et al., 2016), deposition of acidic particles and inorganic nitrogen (e.g., Driscoll et al., 2007), and human health (e.g., Fang et al., 2017). Despite its importance, it is difficult to measure aerosol acidity directly because of the low water content and the high ionic strength in aerosol particles, especially atmospheric aerosols are often in non-ideal states (Mekic and Gligorovski, 2021). In general, the proxy methods and the thermodynamic models are used to estimate it, however, the direct measurement method of aerosol acidity must be developed, because the determination data of aerosol acidity is needed for connecting the estimation results of the thermodynamic models with the realistic atmospheric aerosol acidity. Recently, the previous studies reported several semi-direct methods for aerosol acidity (Li and Jang, 2012; Jang et al., 2020; Rindelaub et al., 2016; Craig et al., 2017, 2018). However, these methods are difficult to widely apply for real atmospheric samples because of various complexities. Therefore, in this chapter, a direct measurement method for aerosol acidity is developed. In order that the new direct measurement method can be widely applied for real atmospheric samples, pH testing paper is selected as the major experimental material, because it is simple to purchase and utilize, and the results of pH testing paper can be detected quickly. Firstly, the color-response accuracy of several kinds of pH testing papers under different ionic strengths is examined to select the optimal pH testing paper. A KNO_3 saturated solution is then used to provide a constant RH of 92%, which enable hygroscopic constituents in the aerosol sample to form an aqueous droplet that possesses a realistic high ionic strength. After selecting the best pH testing paper using the droplet tests, it is examined further to measure the atmospheric aerosol samples.

3.1 Experiments

3.1.1 Screening of pH testing papers

Many kinds of pH testing papers are commercially available from several manufacturers. In this study, six pH testing papers (TP1 to TP6) were examined. Their details are presented in Table 3. To examine the color responses of the pH testing papers, three kinds of salt mixture solutions were prepared according to the major ions often found in aerosol particles. As shown in Table 4, the salt mixture solutions are as follows: SM1 composed of ammonium sulfate, SM2 composed of ammonium sulfate and sodium chloride, and SM3 composed of ammonium nitrate and ammonium bisulfate. Instead of the typical winter aerosol combination of ammonium sulfate and ammonium nitrate, which yield similar results as SM1 and SM2, ammonium bisulfate was used in SM3 to provide low-pH solutions and to test the wide pH range of aerosol particles (from −1 to 5; Pye et al., 2020). All chemicals were >98% purity and manufactured by Wako Pure Chemical Industries Ltd. The solutions of these salt mixtures were prepared with ionic strengths of moderate (0.006 to 0.4 mol kg^{-1}) to high (17.2 to 32.0 mol kg^{-1}), which are referred to as dilute solutions (IS1 and IS2), dense solution (IS3), and saturated solution (IS4). The corresponding mass fraction (ω, %) of each salt solute in the solvent of pure water is also presented in Table 4. The properties of all chemicals for this study are presented in Table 5. The room temperature for the experiments and tests was 25 ℃. The pH testing paper results were compared with the pH measured using a pH meter (LAQUAtwin, pH-11B, Horiba, Japan) to evaluate the color response of the pH testing papers under different ionic strengths.

Table 3. Summary of the examined pH testing papers.

pH testing paper	TP1	TP2	TP3	TP4	TP5	TP6
pH range	1–14	0–6.0	0.5–5.5	4.0–7.0	1.0–3.5	3.6–5.1
Interval scale	1	0.5	0.5	0.3	0.5	0.3
Thickness (mm)	0.1	0.45	0.1	0.1	0.4	0.4
Type	Strips	Strips	Roll	Roll	Strips	Strips
Product code	9.129805	9200	90205	90207	005.3	006.3
Manufacturer	a	b	c	c	d	d

a: Lab Logistics Group GmbH (LLG-Labware); b: Micro Essential Laboratory Inc.;
c: Macherey-Nagel GmbH & Co. KG; d: Johnson Test Papers Ltd.

Table 4. Compositions and ionic strengths of salt mixture solutions.

Salt mixture solution		Ionic strength[a] (mol kg^{-1})			
		IS1	IS2	IS3	IS4
SM1	$(NH_4)_2SO_4$	0.2 (1)[b]	2.4 (10)	6.1 (21)	17.2 (43)
SM2	$(NH_4)_2SO_4$	0.4 (1)	3.8 (10)	8.6 (21)	23.1 (43)
	NaCl	(0.7)	(7)	(13)	(26)
SM3	NH_4HSO_4	0.006 (0.02)	0.06 (0.2)	8.7 (24)	32.0 (49)
	NH_4NO_3	(0.03)	(0.3)	(32)	(65)

[a] Ionic strength was estimated as $\frac{1}{2}\sum m_i z_i^2$, where m and z are the molal concentration (mol kg^{-1} solvent) and the charge number of ion i, respectively.

[b] Values in parentheses show the mass fraction (ω,%) of the salt solute in the solvent pure water.

Table 5. Properties of the salts mentioned in this study.

Salt	DRH, (%, 25 °C)[a, b]	Solubility, (grams per 100 g H_2O, 20 °C)[c]
KNO_3	92	31.6
$(NH_4)_2SO_4$	81	75.4
NH_4HSO_4	40	100
NH_4NO_3	62	192
NaCl	75	35.9
K_2SO_4	97	11.1
Na_2SO_4	84	19.5
KCl	84	34.2

[a] Seinfeld and Pandis (2006).

[b] Lide (1994).

[c] IUPAC (2012).

3.1.2 Testing under realistic high ionic strengths

To further test the color responses of the pH testing papers under realistically high-ionic-strength atmospheric conditions, the aqueous solution droplets were prepared under high RH conditions using the deliquescence of hygroscopic particles. A small amount (ca. 2 mg) of the dry salt mixtures of SM1 and SM2 were placed under high RH in an airtight box (750 cm^3, as shown in Fig. 14) for 5 hours. The RH of the air in the airtight box was maintained at 92% using a saturated solution of KNO_3 due to the high deliquescent relative humidity (DRH) of KNO_3 (Rockland, 1960). The mass of KNO_3 was approximately 40 g, with a corresponding pure water mass of approximately 10 g, and the superficial area of

the KNO_3 saturated solution was approximately 80 cm^2. Because the DRH of all of the dry salt mixtures (SM1 and SM2) were lower than 92%, the dry salt particles could form droplets in the airtight box. Next, the pH testing papers were used to measure the pH of the droplets after quickly opening the airtight box. To prevent drying of the droplets by laboratory air after opening the airtight box, one side of the lid was lifted approximately 30° to allow insertion of the pH testing paper, and the operation was completed within 5 seconds.

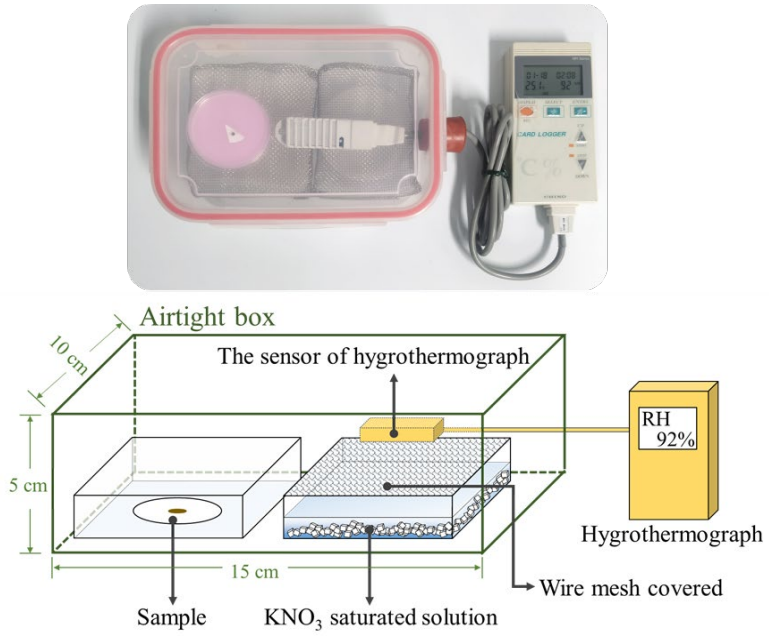

Figure 14. Schematic diagram of the measurement apparatus using pH testing paper for aerosol samples. The RH of the air in the airtight box (750 cm^3) was maintained at 92% by using a KNO_3 saturated solution. A small hygrothermograph sensor was placed inside to monitor the RH and temperature in the airtight box. The sample was held in the 92% RH airtight box to form droplets following hydration. The pH of a resulting droplet was measured using the pH testing paper quickly after the airtight lid was opened.

Considering the influence of temperature on both the pH of pure water (Light, 1984) and the pH of atmospheric aerosols (Tao and Murphy, 2019), the temperature effects of this experiment were investigated by changing the temperature from 15 to 35 °C with 10 °C intervals. The water content of each droplet was also measured via the weighing of water-

absorbent paper (Whatman No. 41; Whatman Paper Ltd, UK). Firstly, this water-absorbent paper was used to absorb different masses of pure water and imaged the wet areas on this paper using a digital camera. Then, the wet area was calculated using ImageJ software (https://imagej.nih.gov/ij/index.html). The correlation between the wet area ($S_{wet\ area}$, mm^2) on the water-absorbent paper and the mass (mg) of pure water is presented in Fig. 15. The regression line in Fig. 15 is expressed as follows:

$$M_{water} = 0.0002S^2_{wet\ area} + 0.03S_{wet\ area}. \quad (2)$$

The water in a droplet in the 92% RH airtight box was also absorbed by the water-absorbent paper. After the wet area on the water-absorbent paper was calculated, the droplet water content was estimated using Eq. (2). Parallel experiments of the water content were conducted six times to determine the average value.

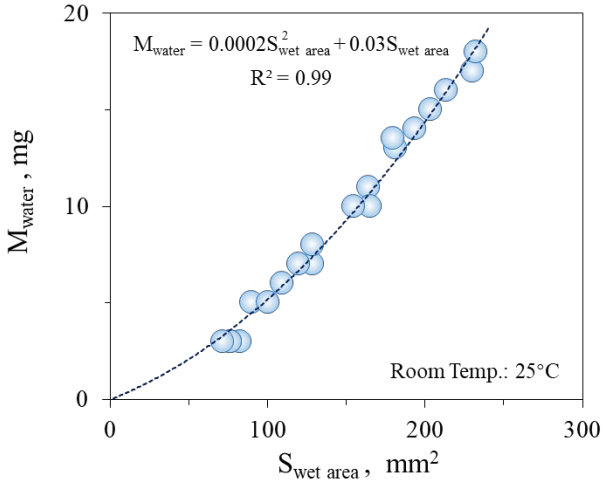

Figure 15. Correlation between the wet area (mm^2) on the water-absorbent paper and the mass (mg) of pure water.

3.1.3 Readout method for the color changes of the pH testing paper

The color of the pH testing papers changes after reaction with the droplet formed from the sample particles when the droplet diameter is greater than 0.7 mm (ca. 0.1 μL). The color response of the pH testing paper does not show differences between the droplet sizes (Fig. 16).

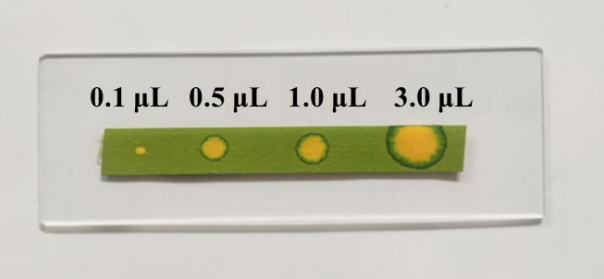

Figure 16. TP3 color responses for different droplet volumes. These droplets were prepared using a micropipette for 0.1, 0.5, 1.0, and 3.0 µL of the dilute solution (IS 1) of SM3.

The colors of the pH testing papers after this reaction and the color scale of the pH indicator supplied by the manufacturer were photographed together in the same image using a digital camera. To reduce the visual error caused by the lightness of the image and human error, a readout method for the pH testing paper color is developed in this study. Recently, several studies have used a MATLAB script to estimate the color–pH relationship based on red, green, and blue (RGB) values (Craig et al., 2018; Li et al., 2020a; Angle et al., 2021). Instead estimating three parameters (RGB), for a simpler method, we applied the hue value of a color (Agoston, 2005). The hue values provide a value on a single-color axis for all colors regardless of lightness and saturation. By using the hue color axis, the color of pH testing paper can be expressed by only one parameter. Compared with the RGB estimation method, the hue value is more preferable for color-based detection (Fitriyah and Wihandika, 2018). The color palette function of the PicPick software (https://picpick.app/en/) was used to extract the hue value. An example color readout is presented in Fig. 17.

As shown in Fig. 18, a calibration curve was created using the pH values as the X-axis and the hue values of the color scale of the pH indicator as the Y-axis. Using this calibration plot, the hue value of the color of the reacted pH testing paper was converted to the pH value of the sample.

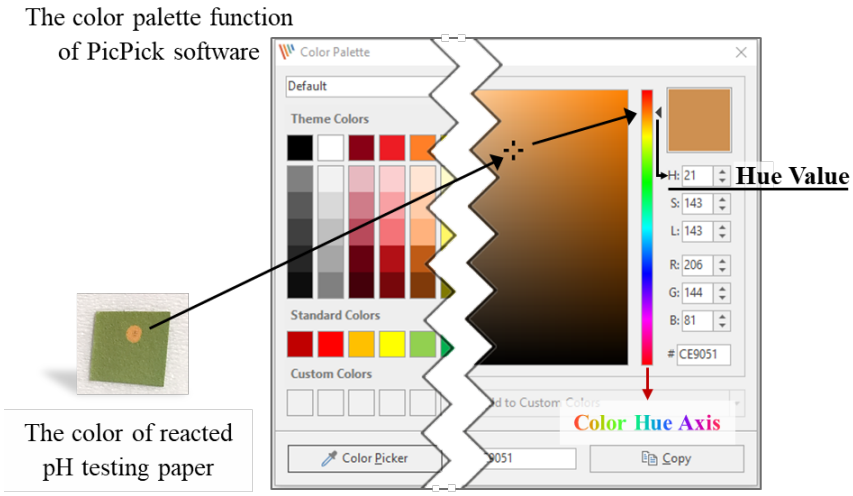

Figure 17. Illustration of obtaining the hue value for the reacted pH testing paper by using the color palette function of PicPick software.

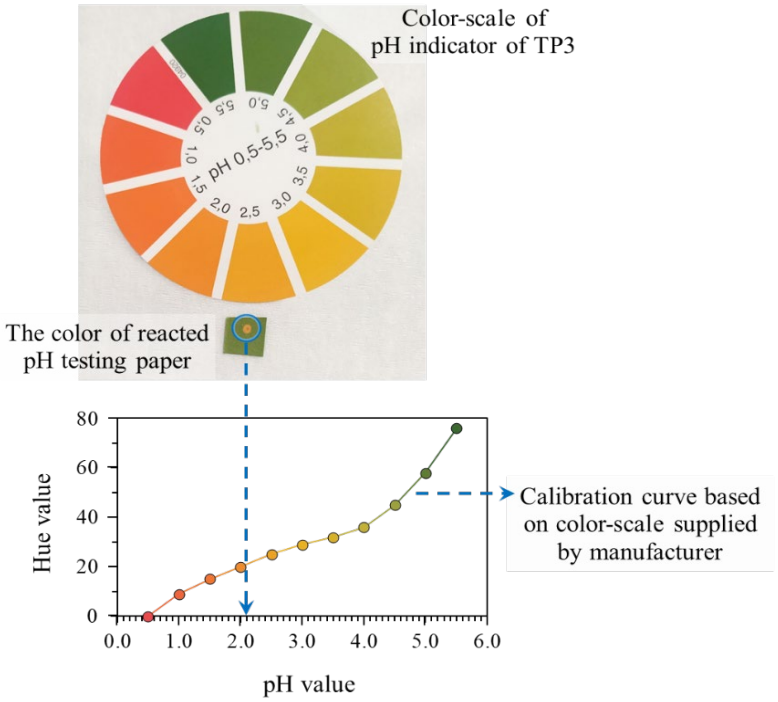

Figure 18. Schematic of the pH estimation from the color of the reaction spot on the pH testing paper. The digital values of the hue for the place of interest were obtained using the color palette function of the PicPick software. The hue values of the color scale for pH indication were used to create a calibration curve. As an example, the pH for the color of the reaction spot shown above is 2.1.

3.1.4 Size-segregated sampling of aerosol particles

The atmospheric aerosol samples were collected using an inertial impactor (Kawakami et al., 2008) on the rooftop of the Environmental Studies Hall of the Higashiyama Campus of Nagoya University (35.16°N, 136.97°E) from October 2019 to January 2020. As mentioned previously, the annual average $PM_{2.5}$ concentration in Nagoya in recent years is approximately 12 μg m^{-3} (https://www.city.nagoya.jp/kankyo/page/0000129706.html). Time-series data of $PM_{2.5}$ concentration during the sampling periods in this study are presented in Fig.19.

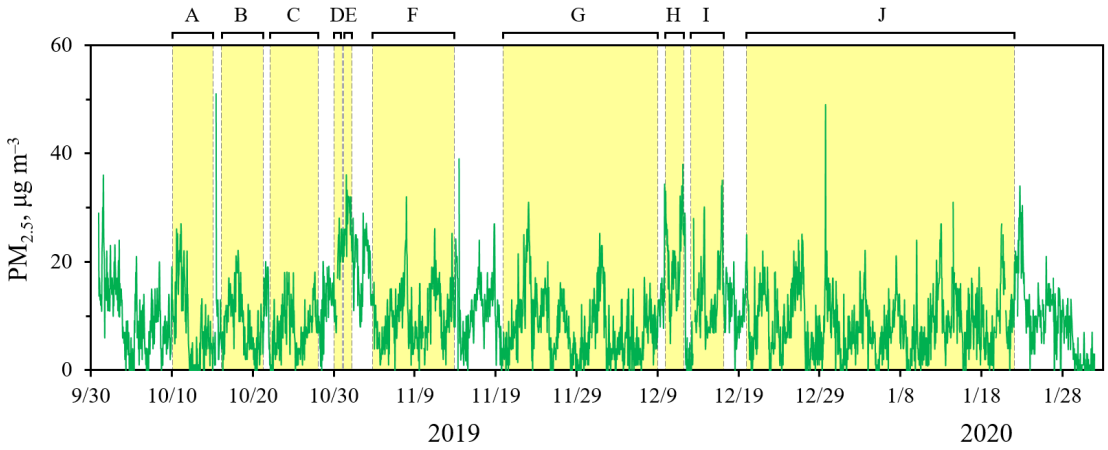

Figure 19. Time series of $PM_{2.5}$ concentrations in Nagoya from October 2019 to January 2020 obtained from Nagoya Air Quality Measurement Station (https://soramame.env.go.jp/). The sampling periods for aerosol particles (with aerodynamic diameters of 0.2 to 2.0 μm) used in this study are shown in the shaded yellow areas.

The inertial impactor has seven and nineteen nozzles for stages 1 and 2, respectively. The estimated aerodynamic 50% cutoff diameters were 2.0 μm for stage 1 (coarse particle sample, >2.0 μm) and 0.2 μm for stage 2 (fine particle sample, 0.2–2.0 μm) at a flow rate of 26 L min^{-1}. The samples were collected on Polytetrafluoroethylene (PTFE) sheets (25 mm diameter; T020A025A, Advantec Toyo Kaisha Ltd.) for both stages. To obtain the different mass accumulations of aerosols, we conducted ten runs of air sampling by

controlling the sampling duration. All sample sheets were stored in air-tight polypropylene tubes and kept in a refrigerator until laboratory tests were conducted.

One spot (Fig. 20) was separated from the sample sheet and placed in the high-RH airtight box for pH measurement to form a hygroscopic droplet. Seven spots from the sample sheets were extracted using 13 mL of pure water overnight. The extracts were analyzed for major ionic constituents (NH_4^+, SO_4^{2-}, NO_3^-, Na^+, Cl^-, Ca^{2+}, Mg^{2+}, and K^+) using ion chromatography (LC-10A modified; Shimadzu Corp.).

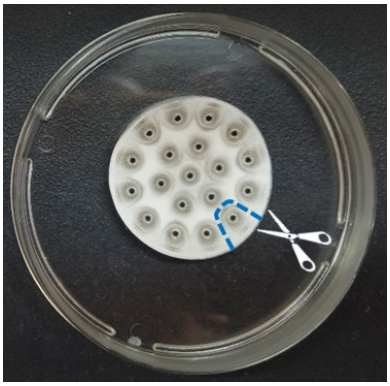

Figure 20. Size-segregated samples of aerosol particles. Both coarse and fine particle samples were collected on PTFE sheets (25 mm diameter). For pH measurements, one spot from the sample sheet was separated and placed in the 92% RH airtight box. Two spots for the coarse particles and seven spots for the fine particles were used for pure water extraction to analyze the major ionic constituents.

3.2 Results and Discussion

3.2.1 Screening results for the pH testing papers

To examine the color responses of the six pH testing papers under different ionic strengths, the pH of the salt mixture solutions was measured using both a pH meter and the pH testing papers. The results of these comparisons are shown in Fig. 21. The pH values of solutions SM1–2 measured using a pH meter were 4.8–5.6. The pH values of the SM3 solutions measured using a pH meter were 0–3.0, which were lower than those of the SM1–2 solutions because of the included NH_4HSO_4. All pH values for the salt mixture solutions increased concomitantly with increasing ionic strength. The pH of the ammonium salt solution depends on the dissociation of H_2O and NH_4^+. The enhanced ionic strength

increases $pK_{NH_4^+}$, thereby decreasing the pH of the solution (Maeda, 2000). Among the six examined pH testing papers, the results of TP3 (diamonds) were the most consistent with the results of the pH meter (Fig. 21). The results of the other pH testing papers were largely different from the pH meter results, especially for higher ionic strengths. For instance, the pH measured by the pH meter was 4.8–5.1 for the saturated solutions (IS4) of SM1–2, while the results determined by the pH testing papers TP2 and TP4 were 2.5–3.0 and 6.1–6.4, respectively. These discrepancies are attributed to functional accuracy of the dye used in the pH testing papers under higher ionic strengths, as discussed by Pye et al. (2020). Therefore, some pH testing papers may provide erroneous results under realistically high-ionic-strength conditions found in atmospheric aerosol particles.

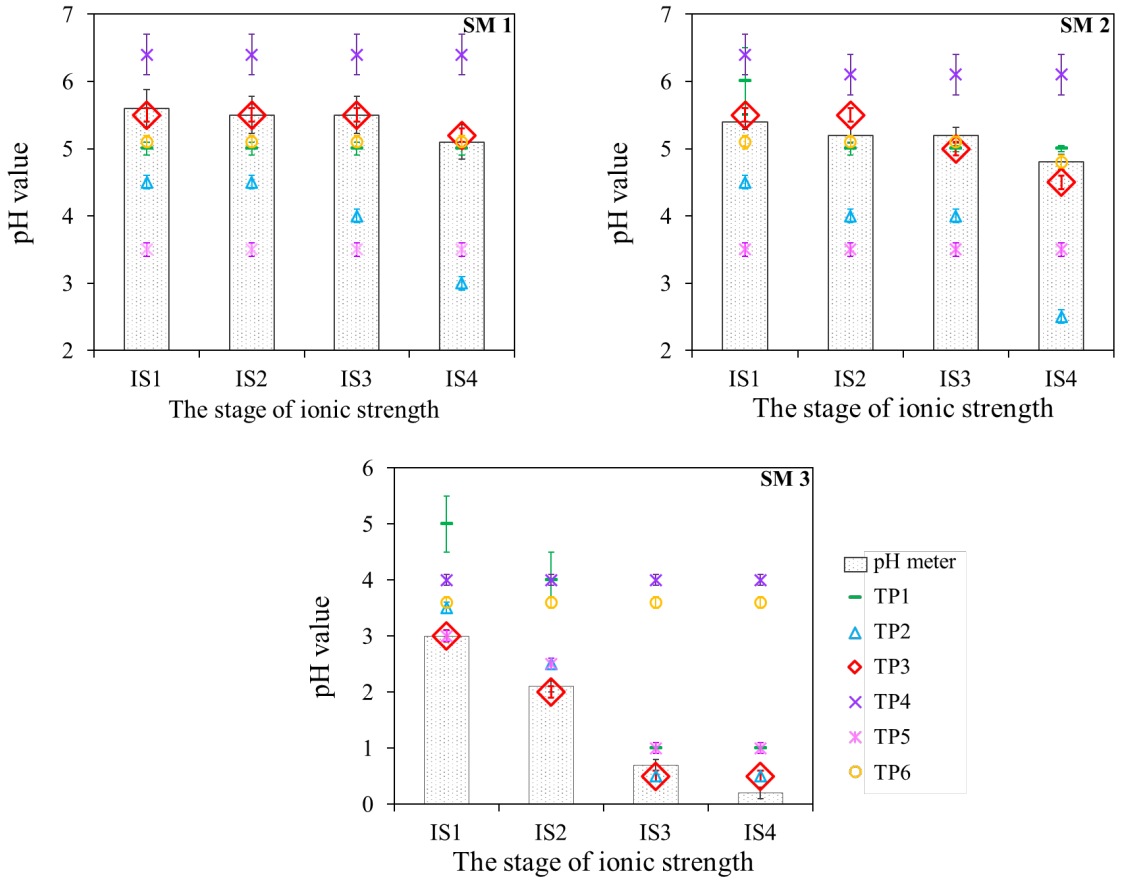

Figure 21. Comparison of the results measured by the pH meter and those by the pH testing papers. The results of the pH testing papers are differentiated using symbols; those of the pH meter are indicated by gray bars. Error bars indicate the standard deviation of three to four repeated measurements.

3.2.2 Test results obtained under realistic high ionic strength

It has been suggested that the ionic strength of water in real aerosol particles is extremely high (Herrmann et al., 2015; Su et al., 2020; Mekic and Gligorovski, 2021). Thus, TP3 was tested further under realistic high-ionic-strength conditions using hygroscopic equilibrium, as described in Section 3.1.2. First, a KNO_3 saturated solution was used to maintain the RH of the air at 92% in an airtight box. The dry salt particles of SM1 and SM2 were permitted to form a droplet, and the pH of the droplet was then measured using TP3. The results of this experiment were pH 3.6–3.7 at 25 °C, approximately 1 pH unit lower than those of the saturated solutions of SM1 and SM2 (4.8–5.1), as shown in Fig. 21. To investigate the reason for this difference in pH between the droplet experiments and the IS1–4 solutions used in Fig. 21, the changes in the droplet pH over time were recorded using 10 μL droplets of the IS3 solutions of SM1 and SM2 instead of the dry salt particles. Moreover, all saturated salt solutions other than KNO_3 were tested at high-RH conditions, including saturated solutions of K_2SO_4, Na_2SO_4, KCl, $(NH_4)_2SO_4$, KNO_3 with $(NH_4)_2SO_4$, and K_2SO_4 with $(NH_4)_2SO_4$. For later experiments using KNO_3 with $(NH_4)_2SO_4$ and K_2SO_4 with $(NH_4)_2SO_4$, a saturated solution of $(NH_4)_2SO_4$ was not mixed with KNO_3 or K_2SO_4, but rather separately placed in the airtight box. The mass of the $(NH_4)_2SO_4$ saturated solution was approximately one-third of that of the KNO_3 or K_2SO_4 saturated solution. The RH of all experimental conditions was higher than 80% (see Table 5). The results of the pH time evolution were divided into two groups: one without $(NH_4)_2SO_4$, which sharply decreased from 4.5 to 3.5 in 4 hours, and the other with $(NH_4)_2SO_4$, which remained at approximately 4.5 for 5 hours, as shown in Fig. 22. The results for KNO_3 and K_2SO_4 with $(NH_4)_2SO_4$ are similar to the pH values of the saturated solutions of SM1 and SM2. The pH changes with time for a NaCl solution and pure water were also measured under experimental conditions similar to those described above using TP3. Although the pH values of these substances were greater than the maximum value (5.5) of the measuring range of TP3, the pH results for both experiments were always greater than 5.5, thus suggesting that no acidic gas existed in the airtight box.

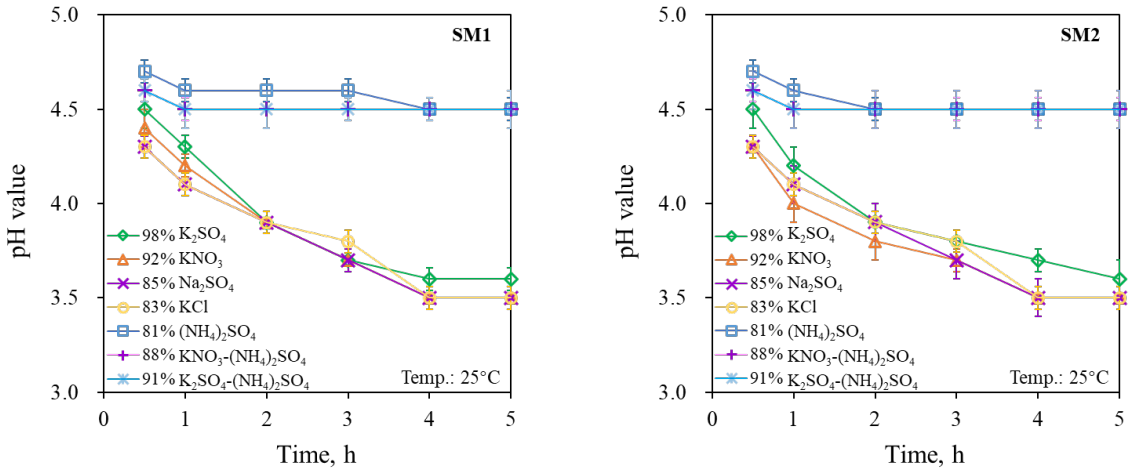

Figure 22. Changes in the droplet pH with time at 25 °C. Each droplet was prepared by using the IS3 solutions of SM1 and SM2. The droplet pH was measured using TP3. The RH of the air in the airtight box was controlled using various saturated salt solutions: K_2SO_4, KNO_3, Na_2SO_4, KCl, $(NH_4)_2SO_4$, KNO_3 with $(NH_4)_2SO_4$, and K_2SO_4 with $(NH_4)_2SO_4$. Error bars indicate the standard deviation of three repeated measurements.

The results of the above experiments suggest that the presence or absence of $(NH_4)_2SO_4$ in the RH-controlling solution influences the droplet pH of SM1 ($(NH_4)_2SO_4$) and SM2 ($(NH_4)_2SO_4$ and NaCl). Considering that the droplets of both SM1 and SM2 contain $NH_4^+{}_{(aq)}$, partitioning between $NH_4^+{}_{(aq)}$ and $NH_{3(g)}$ after the hydration of dry salt under high-RH conditions should be accomplished between the droplet and the air in the airtight box. Because the NH_3 concentration in the airtight box was initially low, the loss of $NH_4^+{}_{(aq)}$ as a consequence of NH_3 evaporation from the droplets may cause the formation of bisulfate in the droplet, as in the following reaction:

$$SO_4^{2-}{}_{(aq)} + NH_4^+{}_{(aq)} \rightarrow HSO_4^-{}_{(aq)} + NH_{3(g)}\uparrow \qquad (R1)$$

Therefore, the experimental conditions without $(NH_4)_2SO_4$ in the RH-controlling solution causes the evaporation of NH_3 from the droplets of SM1 and SM2, thereby decreasing the pH of the droplets. The stable pH results for the droplets that did not contain NH_4^+, such as the NaCl solution and pure water, support the occurrence of a pH decrease due to $NH_4^+{}_{(aq)}/NH_{3(g)}$ partitioning. Therefore, controlling the $NH_4^+{}_{(aq)}/NH_{3(g)}$ equilibrium is important for the pH measurement of these droplets, especially in the case of high NH_4^+ and SO_4^{2-} contents.

Considering that the dissociation constant of many chemicals is temperature-dependent, this study investigated the effects of temperature on the pH of droplets that formed from the dry salt particles of SM1 and SM2 under high RH conditions. Figure 23 presents the droplet pH and the water content of these droplets under different temperatures. Both of these values decreased slightly with increasing temperature. The temperature dependence of ammonium dissociation contributes to the slight decrease in pH. The reduced water content affects the H^+ concentrations in the droplets, which induces a decrease in the droplet pH. Meanwhile, water content can also affect ionic strength in the droplets, resulting in a change in $pK_{NH_4^+}$. For these two reasons, water content has a serious impact on aerosol acidity. Zheng et al. (2020) previously indicated the significant influence of the water content on aerosol pH based on the multiphase buffer theory of aerosol acidity. Moreover, the temperature dependence of H_2O dissociation alters the pH of the droplets. For instance, the pH of pure water slightly decreases from 7.27 to 6.77 as the temperature changes from 10 to 40 °C (Light, 1984). Therefore, the observed decreasing pH with increasing temperature is attributed to the decrease in the water content, the temperature dependence of the H_2O, and ammonium dissociations. According to these results, the temperature utilized during such experiments should be constant.

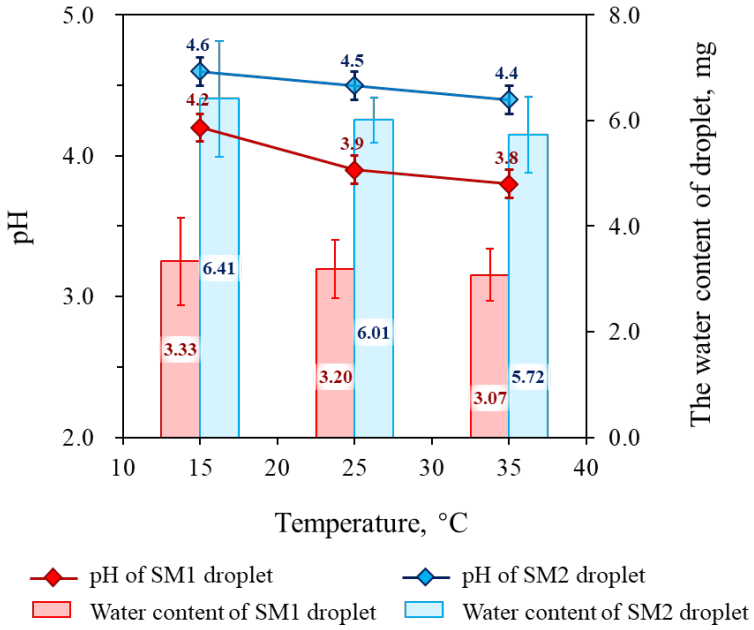

Figure 23. Effects of temperature on the droplet pH measurement and the water content of the droplets formed from the dry salt mixtures under high-RH conditions. The pH values of the droplets from SM1 and SM2 (diamonds) were measured using TP3. The water contents of the droplets were measured using a water-absorbent paper. Error bars indicate the standard deviation of four repeated measurements.

3.2.3 Application of selected pH testing paper to measure the pH of aerosol particles

Using the deliquescence of hygroscopic constituents in a sample, TP3 can be used to measure the pH of a droplet formed from a dry salt mixture under high- and constant-RH conditions. To test the capability of TP3 for measuring the pH of atmospheric aerosol samples, ten different samples were collected with varying amounts of fine particles. One spot of the sample sheet was cut and placed in the high-RH airtight box. Two experimental conditions were set: one in which the KNO_3 saturated solution was used, and another in which the KNO_3 and the separated $(NH_4)_2SO_4$ saturated solution were placed in the airtight box. The temperature was set at the average temperature of the sampling period. The pH of a droplet formed from the collected aerosol particles was measured using TP3. Figure 24(a) presents the results of the droplet pH measured using TP3, where the samples are

marked with letters denoting their sampling periods, as shown in Fig. 19. Among the 10 samples, seven were adequately large such that TP3 measurements could be obtained. Similar results were obtained for both experimental conditions. In the KNO_3 with $(NH_4)_2SO_4$ condition, the pH values of the seven samples ranged from 2.2–2.7, while the results without $(NH_4)_2SO_4$ ranged from 2.1–2.7. As indicated by the red circle in Fig. 24(a), only two samples demonstrated changed pH results between these conditions. Both of these samples provided a higher pH under the KNO_3 with $(NH_4)_2SO_4$ condition, which presumably occurred because the SO_4^{2-} contents (43% and 37% of the total equivalent concentration) in these two samples were higher than the average value across the other samples of 30%. This result suggests that the $NH_{3(g)}$ concentration in the airtight box must be controlled to achieve an appropriate equilibrium, especially for the sample with a high SO_4^{2-} concentration.

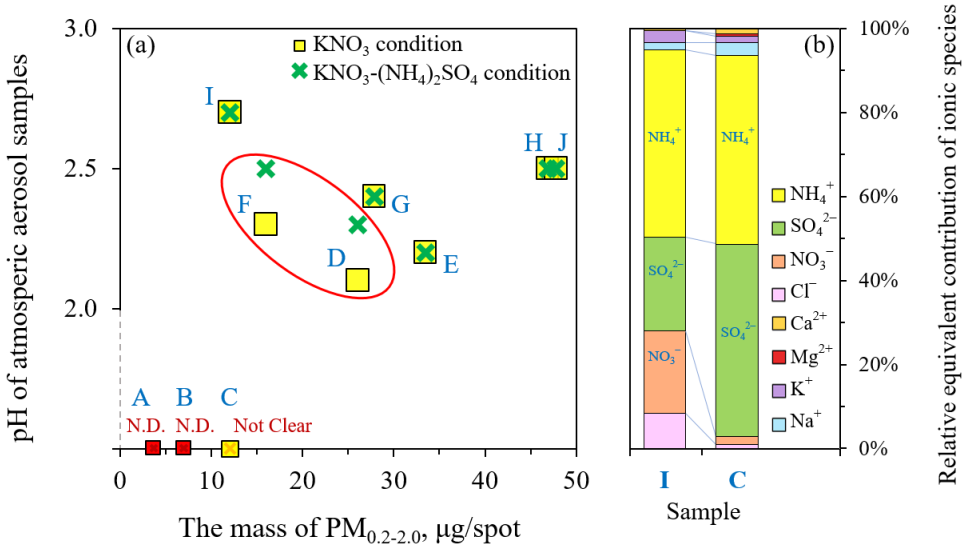

Figure 24. (a) Measurement results of the fine particle samples using TP3 with KNO_3 (yellow squares) and KNO_3 with $(NH_4)_2SO_4$ (green crosses) under experimental conditions to maintain a constant and high RH. Letters in the scatter plot correspond to their sampling periods as shown in Fig. S3 in the Supplementary Material. **(b)** Relative contributions of major ionic species based on the average equivalent concentrations in samples I and C.

The minimum sample amounts of fine particles that can form detectable droplet sizes under high-RH conditions were investigated. In this study, the size range of the aerodynamic diameter of fine particles was 0.2 to 2.0 μm. Assuming the same mass size distribution of typical urban aerosol (Whitby, 1978), the mass of the size range of 0.2 to 2.0 μm ($PM_{0.2–2.0}$; μg m^{-3}) was estimated to be 72% of that of $PM_{2.5}$ (mass concentration (μg m^{-3}) of aerosol particles below 2.5 μm in terms of aerodynamic diameter), as shown in Fig. 25. It also assumed that the ratio of the total major ionic constituents in $PM_{0.2–2.0}$ is the same as that ($R_{2.5}$, 38%) for $PM_{2.5}$ as measured in Nagoya (Nagoya City, 2020, https://www.city.nagoya.jp/shisei/category/53-5-22-8-1-2-0-0-0-0.html). The results of a chemical analysis on a sample sheet of $PM_{0.2–2.0}$ were used to estimate the mass ($M_{0.2–2.0}$; micrograms per sheet) on the sample sheet as follows:

$$M_{0.2\text{-}2.0} = T_{ion} \times 0.72 / R_{2.5}, \quad (3)$$

where T_{ion} (μg) is the total major ionic constituents of $M_{0.2–2.0}$. Because the inertial impactor has 19 nozzles for collecting fine particle samples, 19 sample spots formed on the sample sheet. Therefore, the mass per spot ($M_{0.2–2.0}$ per spot, μg) was obtained as $M_{0.2–2.0}$ divided by 19.

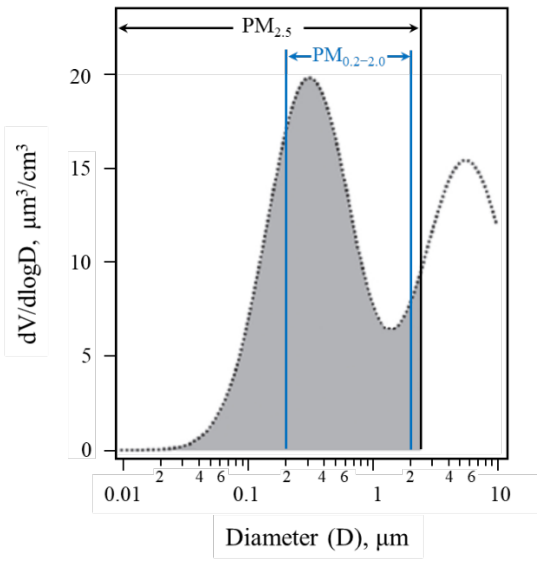

Figure 25. Volume mass size distribution of a typical urban aerosol (gray dotted curve; Whitby, 1978). The shaded area represents the size range of $PM_{2.5}$. According to the area ratio of the $PM_{0.2–2.0}$ and the shaded area for $PM_{2.5}$, the proportion of $V_{0.2–2.0}$ in $PM_{2.5}$ is 72%.

Our method for estimation of the minimum $PM_{2.5}$ requirement can be extended to other sites by using the corresponding $R_{2.5}$, such as 90% in a marine site (Warneck and Williams, 2012) and 30% in Beijing (Wang et al., 2005).

As shown in Fig. 24(a), seven samples with $M_{0.2–2.0}$ per spot values that were larger than 12 μg (T_{ion} > 6.0 μg) formed droplets greater than 0.7 mm in diameter; therefore, their pH values were successfully measured using TP3. However, when $M_{0.2–2.0}$ per spot was ca. 12 μg (as indicated by "I" and "C" in Fig. 24(a)), the color response of TP3 was not clearly observable. The color change of the pH paper for sample I was clearly visible, while that for sample C was unclear. This difference may be attributed to the difference in the major ionic compositions of these samples. As shown in Fig. 24(b), the equivalent ratio of NH_4^+, SO_4^{2-}, and NO_3^- for sample I was close to 2:1:1, and these ions in the sample existed in the forms of NH_4HSO_4 and NH_4NO_3. In contrast, the equivalent concentration of NO_3^- in sample C was much lower than those of NH_4^+ and SO_4^{2-}. The equivalent ratio of NH_4^+ and SO_4^{2-} was close to 1:1 for sample C, suggesting that $(NH_4)_2SO_4$ was the major component in this sample. According to the simple mixing rule of the hygroscopicity parameter (κ), the κ parameter of the mixed components of NH_4NO_3 and NH_4HSO_4 (volume ratio ≈ 1:1) is 0.62, slightly higher than that of $(NH_4)_2SO_4$ (0.53) at ~90% RH (Petters and Kreidenweis, 2007; Carrico et al., 2010; Liu et al., 2014), the diameter of the droplet formed from sample I was larger than that from sample C. Therefore, even if the value of $M_{0.2–2.0}$ per spot is 12 μg, the resulting droplet may be smaller than the detectable size, depending on the composition.

3.2.4 Comparison with previous methods and future direction of our method

The existing methods for the pH measurements of aerosol samples have disadvantages, including complexity and various limitations. The C-RUV method (Li and Jang, 2012; Jang et al., 2020) requires a complex calculation to obtain the H^+ concentration; it partially relies on the parameters estimated from the E-AIM model, such as the density of the solution and water mass fraction of the total aerosols. The Raman microspectroscopy method (Rindelaub et al., 2016; Craig et al., 2017) is limited to samples of laboratory-generated aerosol particles composed of a single acid and its conjugate system. In contrast, the newly-method developed in this study can be applied in many laboratories without expensive and

complicated equipment. Although the previous method for pH testing paper developed by Craig et al. (2018) showed the potential for aerosol pH measurement, uncertainty exists because of the lack of stringent examinations of pH testing papers. As the results of this study demonstrated that only one testing paper was suitable because of high ionic strength conditions.

The above comparison demonstrates that the newly-method is more convenient and reliable for wide application. However, uncertainties related to the effects of $NH_4^+{}_{(aq)}/NH_{3(g)}$ equilibrium may occur during sample storage and hydration in the airtight box, as discussed in Sections 3.2.2 and 3.2.3. Ideally, the NH_3 concentration in the airtight box should be controlled at the average value of the sampling period, and doing so will ensure that the proposed method provides reliable results.

3.3 Chapter summary

A direct measurement method for the acidity of aerosol samples was developed using pH testing paper in this chapter. The color responses of six pH testing papers were examined firstly using salt solutions with different ionic strengths. By testing with artificial salt mixtures that are often found in the atmosphere, the best pH testing paper was identified and further tested using hygroscopic equilibrium under high-RH conditions with a KNO_3 saturated solution. Experiments for measuring the pH of atmospheric aerosol samples were conducted to determine the minimum amount of aerosol particles required by changing the sampling duration, which indicated that approximately 12 μg per spot is the minimum required value, depending on the major ionic constituents. Compared with other existing methods used to determine aerosol acidity, the proposed method is more convenient and reliable for wide application in many laboratories without expensive and complicated equipment. The aerosol acidity data provided by this method is useful in understanding pH-dependent chemical processes, and it may serve to connect idealized thermodynamic models with the actual acidity of aerosol particles.

Chapter 4: Characterization of aerosol acidity using the pH testing paper method combined with the E-AIM IV model

Since the proxy methods and the thermodynamic models are widely used in inferring aerosol acidity, most of the current understandings of aerosol acidity remain in the idealized scenarios. However, aerosol particles are often in non-ideal state because of the high ionic strength and low water content (Mekic and Gligorovski, 2021; Wei et al., 2018). The difference between the estimation results (ideal state) and the acidity of atmospheric aerosol particles (un-ideal state) is important for improving models to present more reliable analysis and prediction. However, only recently, the direct measurement methods of aerosol acidity become available and need further development before routine and general application. Given the lack of direct measurement data of aerosol acidity, the comparison of aerosol acidity between estimated by the thermodynamic models and detected by the direct measurement methods has not been implemented yet. Therefore, in this chapter, the results of the previous two chapters (Chapter 2 and 3) are compared to reveal the difference between simulations and directly measured values, thereby characterizing aerosol acidity more reliably and making recommendations for improving the thermodynamic model estimation and the direct measurement method.

4.1 Comparison of aerosol acidity values estimated the E-AIM IV model and the pH testing paper method

The pH testing paper method was used to measure the acidity of the fine particle samples collected in Nagoya from December 2019 to January 2020. As shown in Fig. 24(a), their pH (pH_{meas}) was 2.1–2.7, with the average of 2.4. It is quite different from the estimated results of E-AIM IV model in Chapter 2, that is the pH_{ISF} in 2017–2018 winter in Nagoya ranges from 4.42–5.12 with the average of 4.80. Although the results indifferent years have difference, the pH_{ISF} of 2017–2018 is approximately 2.4 pH units higher than the pH_{meas} of 2019–2020, that is, the H^+ concentration converted from pH_{ISF} is approximately $10^{2.4}$ lower than that converted from pH_{meas}. The reason for this difference should be investigated to refine model estimation or direct measurement method.

Herein, the E-AIM IV model is used to estimate pH_{IS} based on the ionic analysis results of 2019–2020 fine particle samples with ambient temperatures in the same sampling periods and the RH of 92%. As discussed previous, the NH_3 data is crucial in the model estimation. Thus, the input NH_3 concentration was assumed at (1) the ambient concentrations in the atmosphere during each sampling period ($NH_{3\text{-}Amb}$) which measured by the MF analytical system (see Sect. 2.1.1); (2) the average (30 ppb) of the empirical concentration in the laboratories (Li and Harrison, 1990; Li et al., 2020b).

Figure 26 presents the comparison between the direct measurement method results (pH_{meas}) and the E-AIM IV model estimated results (pH_{IS}), and colored by the ratio of $[NH_4^+]_{modeled}/[NH_4^+]_{measured}$.

Among the estimated results with three assumptions of input ammonia (30 ppb, $NH_{3\text{-}Amb}$, and no-ammonia), the best correlation (R^2=0.90) between pH_{ISF} and pH_{meas} is appeared when the input ammonia is $NH_{3\text{-}Amb}$, while no correlation (R^2=0.08) is found when the input ammonia is 0. As the ratio of $[NH_4^+]_{modeled}/[NH_4^+]_{measured}$ indicated by the color in Fig. 26, $[NH_4^+]_{modeled}$ in the assumption of input ammonia at $NH_{3\text{-}Amb}$ is closest to $[NH_4^+]_{measured}$. It suggests $NH_{3\text{-}Amb}$ is best match for the NH_4^+ concentrations of aerosol particle samples so that the gas/particle partitioning of $NH_4^+/NH_{3\text{-}Abm}$ in E-AIM model calculation is closer to the NH_4^+/NH_3 partitioning in the airtight box. In contrast, when input NH_3 is 30 ppb (inverted triangles), the ratio of $[NH_4^+]_{modeled}/[NH_4^+]_{measured}$ is higher than 1.0, indicating the model simulated results of NH_4^+ is high. As a result, the estimated pH_{IS} used the input NH_3 of 30 ppb is overestimate. Additionally, without input NH_3, the estimated pH_{IS} (hexagons) is scattered. All the results display again that the NH_3 data is important for the model estimation of aerosol acidity and advises that further study of controlling the NH_3 concentration in the airtight box should consider according to the $NH_{3\text{-}Amb}$ data.

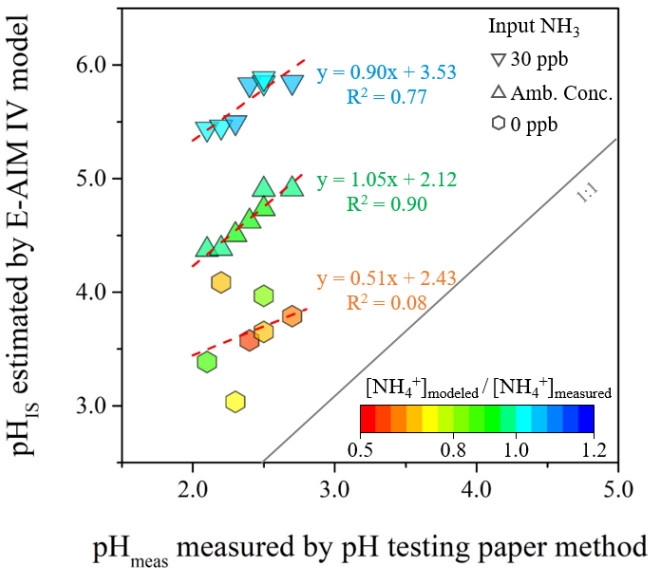

Figure 26. Comparison of the measured results by the pH testing paper method and the estimated results by the E-AIM IV model with three assumptions of NH_3 including the average concentration in the laboratory of 30 ppb, the average concentration of ambient ammonia during each sampling period, and no-ammonia. Colors indicate the ratio of the estimated NH_4^+ to the measured NH_4^+ ($[NH_4^+]_{modeled}/[NH_4^+]_{measured}$).

However, all the estimation results in Fig. 26 are higher than the measurement results. For example, when the $NH_{3\text{-}Amb}$ was input into E-AIM model, the pH_{ISF} was 2.23 pH units higher than pH_{meas} on average. Considering the significant correlation between pH_{meas} and pH_{IS} used input $NH_{3\text{-}Abm}$, the reason of the difference is probably because of the different equations of in situ pH. In the analysis so far, only the Eq. (1) defined on a mole fraction concentration scale recommended by the developers of E-AIM model (Wexler and Clegg, 2002; Friese and Ebel, 2010) was used to calculate pH_{IS}. However, in fact, the original definition of pH was pH = – log (a_H), where a_H is the activity of H^+ (Stumm and Morgan, 1996). Except Eq. (1), this original definition of pH can be transformed into the two other equations according to the definitions gave by the International Union of Pure and Applied Chemistry (IUPAC) as follows (Pye et al., 2020; Jia et al., 2018b):

on a mole fraction scale, $\mathrm{pH}_f = -\log_{10}(a_{fH}) = -\log_{10}(f_H x_H)$, (1)

on a molarity scale, $\mathrm{pH}_c = -\log_{10}(a_{cH}) = -\log_{10}(\frac{\gamma_H c_H}{c^0})$, (4)

on a molality scale, $\mathrm{pH}_m = -\log_{10}(a_{mH}) = -\log_{10}(\frac{\gamma_H m_H}{m^0})$, (5)

where a_i in the three equations denotes the activity of H^+, f_H, γ_H, and y_H stand for the activity coefficients on different standard states. The x_H in Eq. (1) is the mole fraction of H^+ calculated as $x_H = \frac{n_H}{\sum_j n_j}$ (where n_H is the moles of H^+, and $\sum_j n_j$ is the summation of all solution species *j*, including liquid water). The c_H in Eq. (4) represents the molarity of H^+ (mol dm^{-1} solution, moles of H^+ ion per cubic decimeter of aqueous solution), c^0 is the unit molarity (=1 mol dm^{-3} solution). The m_H in Eq. (5) denotes the molality of H^+ (mol kg^{-1}, moles of H^+ ion per kilogram of solvent, typically pure water), m^0 is the unit molality (=1 mol kg^{-1} solvent).

The Eq. (1) is the application of mole fraction scale, which is suitable for expressing deviations from ideality because it considers all the ionic species in the solution (Stumm and Morgan, 1996). That is probably the reason why it was recommended in E-AIM model (Wexler and Clegg, 2002; Friese and Ebel, 2010)). The Eq. (4) is an operational definition endorsed by the IUPAC based on the work of pH determination of the standard buffer (Covington et al., 1985; Stumm and Morgan, 1996). In 1997, the IUPAC improved the calculation formula of pH definition, that is Eq. (5) (IUPAC, 1997). The results of Eq. (4) and (5) is similar, and the difference is < 0.02 pH unit which can be ignored in the estimation of aerosol pH (Pye et al., 2020). Because of the difference between the units of mole fraction and molality (or molarity), the difference between Eq. (1) and Eq. (4–5) cannot be neglected. In 1 kg aqueous solvent contains 55.5 mole of water (Stumm and Morgan, 1996). The difference of H^+ molality (or molarity) concentration converts to H^+ mole fraction is approximately $\frac{1}{55.5}$. As a result, the difference between pH_f and pH_m (or pH_c) is 1.74.

All the parameters except c_H in Eq. (4) can be obtained from the output of E-AIM model directly. The value of c_H can be converted by using m_H divided by the density of pure water (assuming the solvent in aerosol particles is pure water). Until now, there is no

firm conclusion to indicate the most suitable equation of in situ pH in the application of E-AIM model.

Figure 27 presents the comparison between the results calculated by the definition formulas of pH_f, pH_m, and pH_c based on the input data of the ionic concentrations of 2019–2020 fine particles, the ambient temperatures and the ambient NH_3 concentrations in the same sampling periods, and the RH of 92%. All the estimated results (pH_f, pH_m, and pH_c) presented the same strong correlation (R^2=0.90) with pH_{meas}. The results of pH_m (red squares) and pH_c (yellow diamonds) display the same values. Their values are closer to the pH_{meas} values than the pH_f values (blue triangles). That is the calculated results by the pH definition of H^+ molality (or molarity) concentration are quite similar to the measured results by the pH testing paper method. It might be because both the pH_m (or pH_c) definitions and the pH testing papers are related to the work of pH determination of the standard buffer (Stumm and Morgan, 1996; Atkins, 2000). Considering the similar results, in the future application of E-AIM model for the estimation of aerosol pH, the calculation formula of the pH_m (or pH_c) definitions should consider to be used. Additionally, the remaining difference between of pH_m (or pH_c) and pH_{meas} is 0.5 pH unit on average. It might be because of the lack of NH_3 in the airtight box of the pH testing paper method. Or might be the uncertainty in the E-AIM model, such as the influence of the nonvolatile cations of K^+, Ca^{2+} and Mg^{2+} is not calculated (Guo et al., 2018).

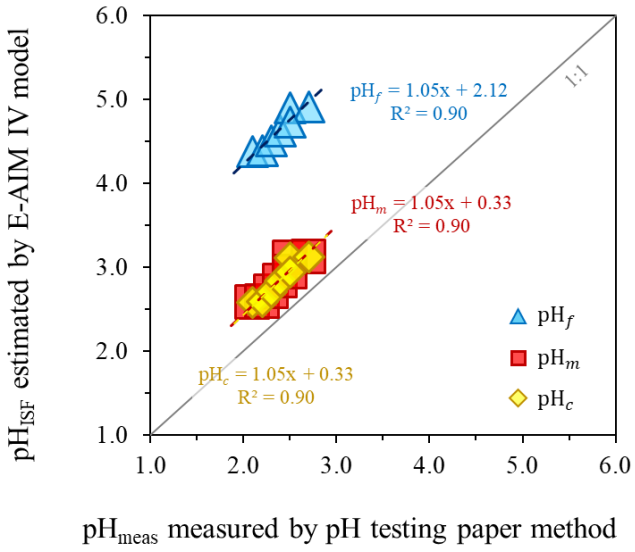

Figure 27. Comparison of the estimation results (pH_{ISF}) of E-AIM IV model and the measured results (pH_{meas}) of pH testing paper method. The pH_{ISF} is calculated according to three different definition equations and indicated by pH_f, pH_m, and pH_c, which respectively represent the mole fraction scale, the molality scale, and the molarity scale.

Furthermore, the pH_{ISF} in Nagoya during 2017–2018 is recalculated by using Eq. (4) that is 1.94–3.63, with the average of 2.70 ± 0.39. Similar results were observed in Canada (the average pH_{ISF} is 2.45) where air pollution is slight (Tao and Murphy, 2019), suggesting that aerosol particles present high acidity even in the less-polluted regions. The summer average of pH_{ISF} in Nagoya is 2.31 ± 0.39, and the winter average is 3.05 ± 0.15. Their difference is approximately 0.74 pH unit. In Canada, the difference between summertime and wintertime is approximately 1 pH unit (Tao and Murphy, 2019). In another report in Beijing (Ding et al., 2019), the season variation of aerosol pH was also observed by the estimation of ISORROPIA II based one-year data including the $NH_{3(g)}$ concentration. The difference of aerosol pH between summertime and wintertime in Beijing is 0.7 pH unit. However, because the higher concentrations of major ions (the concentrations of NH_4^+, and SO_4^{2-}, and NO_3^- were 408 nmol m^{-3}, 80 nmol m^{-3}, and 219 nmol m^{-3}, respectively), the aerosol pH presented the high value of 4.25 on average. As discussed in Fig.13(a) in Section 2.2.4, the sensitivity tests of ionic concentrations effect on pH_{IS} showed that all the ionic concentrations increased leaded to the increase of pH_{IS}. Therefore, with the improving

of air pollution, aerosol pH will decrease in the currently polluted areas. The seasonal variation of aerosol pH in these studies also indicates that the dominant driving factor of aerosol pH is ambient temperature. Also, according to the seasonal variation of aerosol pH, the haze event in summertime might be associated to the decrease of aerosol pH, because the acid-catalyzed reactions of the SOA formation occur frequently in high acidity condition (Surratt et al., 2007, 2010; Han et al., 2016).

On the other hand, it is noteworthy that the $[H^+]_{strong}$ discussed in Section 2.2.1 also presents a similar seasonal variation. However, when it is converted back to the pH of extracts, the difference between summer and winter is only 0.23 pH unit. The great dilution in the extract process of aerosol filter samples results in the uncertainty of H^+ concentration, which causes the proxy method is difficult to obtain reliable results for aerosol acidity, for example, the pH difference between summer and winter. It further illustrates that the results of proxy method are incomplete in terms of aerosol acidity. In future studies, the proxy method should be avoided to be used.

4.2 Discussion of the dominant factors affecting aerosol acidity

Among various meteorological factors, temperature and relative humidity (RH) have the most direct effect on aerosol acidity. Most of Henry's law constants and the dissociation constants of acids and bases are depended on temperature (Seinfeld and Pandis, 2016; Atkins et al., 2000). The change of temperature will directly change the H^+-related thermodynamic equilibriums, and then affect aerosol acidity. In addition, the change of temperature has an influence on the H^+ concentration of aerosol particles because of the liquid water content change with temperature. Another important meteorological factor, RH, strongly affects the hygroscopic growth of aerosol particles (Cruz and Pandis, 2000; Gysel et al., 2002). The aerosol particles with fixed chemical compositions will increase its liquid water content with the increase of RH (Gysel et al., 2002; Topping et al., 2005), and the H^+ concentration will be consequently diluted.

Although some studies have shown that RH has a strong impact on aerosol acidity (Zhou et al., 2012), the E-AIM model estimation and sensitivity test results of Nagoya do not show a significant effect of RH. It might be associated with the low air pollution in Nagoya. Murphy et al. (2017) demonstrated that the RH effect on aerosol acidity increases

significantly when SO_4^{2-} concentration is higher than ca. 100 nmol m^{-3}. However, the annual average concentration of SO_4^{2-} in Nagoya is only 25.2 nmol m^{-3}. For this reason, as analyzed in Section 2.2.4, the temperature effect on aerosol acidity is significant while the RH effect is not exhibited. In Section 3.2.2, although the concentration of SO_4^{2-} in the droplets of SM1–2 is higher than 100 nmol m^{-3}, a slight effect of temperature on droplet pH is still observed under the fixed RH of 92%. Moreover, the water content of droplets also changes slightly with temperature, which is consistent with the sensitivity test results in Section 2.2.4. Therefore, temperature is substantially impacting aerosol acidity, and the major pathway of temperature effect is by changing the liquid water content.

On the other hand, Weber et al. (2016) reported that aerosol acidity remains high level over a long time despite the decrease of atmospheric sulfate concentration because of the buffering effect of the partitioning of NH_3/NH_4^+. This buffering effect has been proved to be related to aerosol liquid water content (Zheng et al., 2020). Thus, aerosol liquid water content is important parameter in the studies of aerosol acidity.

As discussed in Section 3.2.3, the change of the liquid water content is associated with the hygroscopic components. The different contributions of hygroscopic components in particle samples lead to the droplets with different water content, such as the case of sample #1 and #2. Therefore, the influence of hygroscopic components on aerosol liquid water content might be another important mechanism for aerosol acidity change. As the major hygroscopic components, the importance of ammonium, sulfate, and nitrate has also been indicated in Section 2.2.4. Further work investigating the change of hygroscopic components, especially ammonium, sulfate, and nitrate, is needed to supplement the mechanism of aerosol acidity change, so that a more reliable prediction of aerosol acidity can be obtained.

4.3 Chapter summary

By comparing the estimated results of the E-AIM IV model and the direct measured results of the pH testing paper method, the suitable definition of in situ pH in the estimation of E-AIM model is pointed out that is the pH definition on the molality (or molarity) scale. The pH_{ISF} of Nagoya during 2017–2018 is recalculated that ranges from 1.94 to 3.63, with the average of 2.70 ± 0.39, suggesting that aerosol acidity is high despite less air pollution.

Meanwhile, the comparison also indicates that controlling NH_3 concentration in the airtight box is important for the pH testing paper method. The NH_3 concentration in the airtight box should be controlled at the same concentration of ambient ammonia in the atmosphere. Additionally, the dominant factors affecting aerosol acidity are temperature proved by both model estimated results and direct measurement data. The hygroscopic components of ammonium, sulfate, and nitrate are also crucial for aerosol acidity due to the effect on the aerosol water liquid content. Their proportion change should be investigated further to supplement the mechanism of aerosol acidity change.

Chapter 5: Summary and Conclusions

Aerosol acidity plays an important role in atmospheric science that impacts many atmospheric chemical reactions, ecosystem health, and human health. Despite decades of research on aerosol acidity recently, some issues are still unclear, especially the long-term variation characteristics and dominant driving factor(s). This thesis first investigated the variation characteristics aerosol acidity and its driving factors by the forward mode of E-AIM model based on data obtained from continuous observations of NH_3, HNO_3, and ionic constituents of fine particles (<1.9 μm) conducted in Nagoya during 2017–2018. Then, a direct measurement method of aerosol acidity was developed to provide comparable direct measurement data that can connect the estimation results of E-AIM model to realistic atmospheric aerosol. The major results of this thesis can be summarized as follows.

The E-AIM model simulates aerosol inorganic behaviors which take place in the atmosphere, thus, the estimation results were marked with "in situ". Base on the output of E-AIM IV model, including the activity coefficient and the molality concentration of H^+, in situ pH (pH_{IS}) was calculated. It ranged from 1.94 to 3.63, with the average of 2.70 ± 0.39. The highest value (3.63) appeared during a typhoon period when strong southern winds brought huge amounts of sea salt particles (Na^+ and Cl^-). An obvious seasonal variation was presented that low in summer (an average of 2.31 ± 0.39) and high in winter (an average of 3.05 ± 0.15). It significantly correlated with ambient temperature (R^2=0.83, excluding the highest value of 3.63), suggesting that it was the major factor driving the seasonal variation of pH_{IS}. The derivative of pH_{IS} dependence on temperature indicated that increasing temperature by 2.5 °C decreases the pH unit by 0.1.

Further, various sensitivity tests conducted using E-AIM IV were applied to assess factors affecting pH_{IS} in Nagoya by changing them one-by-one while fixing the other factors. The results showed that the temperature effect was apparent only in cases below the threshold SO_4^{2-} concentration (ca. 126 nmol m^{-3} in case of Nagoya), and the temperature dependence of the aerosol liquid water content was an important moderator for the temperature effect on aerosol acidity. The sensitivity tests of the major ionic species showed that the concentrations of SO_4^{2-} and NH_4^+ had a strong effect on pH_{IS}.

To provide a comparison data for the model estimation results, a direct method of aerosol acidity is needed. Based on several rigorous exams, the pH testing paper method was developed by using hygroscopic equilibrium under high relative humidity, and applied to measure the pH of atmospheric aerosol samples. The application results showed that this method requires more than approximately 12 μg $spot^{-1}$ (aerosol particles presented 19 spots in the sample filter) of fine particles. Compared with previous methods, it is simpler, more convenient, and reliable for wide application without excess dilution in practice.

By compared the estimation results of E-AIM model and the measurement results of pH testing paper method, temperature was identified as the dominant driving factor of aerosol acidity, its effect on aerosol acidity was related to the change of liquid water content with temperature. Moreover, the hygroscopic components of ammonium, sulfate, and nitrate also had influence on aerosol acidity, presumably because the relationship between their hygroscopic ability and the liquid water content.

This thesis concluded that aerosol acidity remains high level even in a less-polluted area, and the variation of aerosol acidity is mainly dependent on the temperature change. Additionally, this thesis indicated the most suitable pH definition for estimating aerosol acidity in the application of E-AIM model. Also, a direct measurement method of aerosol acidity was developed. These research approaches can be applied to related studies for improving the understanding of acidity-dependent chemical processes and the predictive capability of models focused on ecosystem and human health.

References

Adams, P.J., Seinfeld, J.H., Koch, D.M., 1999. Global concentrations of tropospheric sulfate, nitrate, and ammonium aerosol simulated in a general circulation model. J. Geophys. Res.-Atmos. 104, 13791–13823.

Agoston, M.K, 2005. Computer graphics and geometric modeling. London: Springer, p. 301.

Ahrens, L., Harner, T., Shoeib, M., Lane, D.A., Murphy, J.G., 2012. Improved characterization of gas–particle partitioning for per- and polyfluoroalkyl substances in the atmosphere using annular diffusion denuder samplers. Environ. Sci. Technol. 46, 7199–7206.

Amann, M., Kiesewetter, G., Schöpp, W., Klimont, Z., Winiwarter, W., Cofala, J., Rafaj, P., Höglund-Isaksson, L., Gomez-Sabriana, A., Heyes, C., Purohit, P., Borken-Kleefeld, J., Wagner, F., Sander, R., Fagerli, H., Nyiri, A., Cozzi, L., Pavarini, C., 2020. Reducing global air pollution: the scope for further policy interventions. Philos. Trans. R. Soc., A. 378 (2183), 20190331.

Angle, K.J., Crocker, D.R., Simpson, R.M., Mayer, K.J., Garofalo, L.A., Moore, A.N., Mora Garcia, S.L., Or, V.W., Srinivasan, S., Farhan, M., Sauer, J.S., Lee, C., Pothier, M.A., Farmer, D.K., Martz, T.R., Bertram, T.H., Cappa, C.D., Prather, K.A., Grassian, V.H., 2021. Acidity across the interface from the ocean surface to sea spray aerosol. Proc. Natl. Acad. Sci. U. S. A. 118 (2), e2018397118.

Ansari, A.S., Pandis, S.N., 1998. Response of inorganic PM to precursor concentrations. Environ. Sci. Technol. 32, 2706–2714.

Appel, B.R., Tokiwa, Y., Haik, M., 1981. Sampling of nitrates in ambient air. Atmos. Environ. 15 (3), 283−289.

Atkins, P.W., 2000. Atkins' Physical Chemistry. New York: Oxford University Press, Chapter 7, 8, 9 10, 25, and 26.

Bae, M.S., Demerjian, K.L., Schwab, J.J., Weimer, S., Hou, J., Zhou, X., Rhoads, K., Orsini, D., 2007. Intercomparison of Real Time Ammonium Measurements at Urban and Rural Locations in New York. Aerosol Sci. Technol. 41, 329–341.

Behera, S.N., Cheng, J., Huang, X., Zhu, Q., Liu, P., Balasubramanian, R., 2015. Chemical composition and acidity of size-fractionated inorganic aerosols of 2013-14 winter haze in Shanghai and associated health risk of toxic elements. Atmos. Environ. 122, 259−271.

Bobbink, R., Hicks, K., Galloway, J., Spranger, T., Alkemade, R., Ashmore, M., Bustamante, M., Cinderby, S., Davidson, E., Dentener, F., Emmett, B., Erisman, J.W., Fenn, M., Gilliam, F., Nordin, A., Pardo, L., De Vries, W., 2010. Global assessment of nitrogen deposition effects on terrestrial plant diversity: a synthesis. Ecol. Appl. 20 (1), 30–59.

Covington, A.K., Bates, R.G., Durst, R.A., 1985. Definitions of pH scales, standard reference values, measurement of pH, and related terminology. Pure Appl. Chem., 57, 531–542.

Carrico, C.M., Petters, M.D., Kreidenweis, S.M., Sullivan1, A.P., McMeeking, G.R., Levin, E.J.T., Engling, G., Malm, W.C., Collett Jr, J.L., 2010. Water uptake and chemical composition of fresh aerosols generated in open burning of biomass. Atmos. Chem. Phys. 10 (11), 5165−5178.

Cheng, C., Wang, G., Meng, J., Wang, Q., Cao, J., Li, J., Wang, J., 2015. Size-resolved airborne particulate oxalic and related secondary organic aerosol species in the urban atmosphere of Chengdu, China. Atmos. Res. 161, 134−142.

Clegg, S.L., Brimblecombe, P., Wexler, A.S., 1998. Thermodynamic model of the system H^+−NH_4^+−SO_4^{2-}−NO_3^-−H_2O at tropospheric temperatures. J. Phys. Chem. A. 102 (12), 2137−2154.

Craig, R.L., Nandy, L., Axson, J.L., Dutcher, C.S., Ault, A.P., 2017. Spectroscopic determination of aerosol pH from acid-base equilibria in inorganic, organic, and mixed systems. J. Phys. Chem. A. 121 (30), 5690−5699.

Craig, R.L., Peterson, P.K., Nandy, L., Lei, Z., Hossain, M.A., Camarena, S., Dodson, R.A., Cook, R.D., Dutcher, C.S., Ault, A.P., 2018. Direct determination of aerosol pH: size-resolved measurements of submicrometer and supermicrometer aqueous particles. Anal. Chem. 90 (19), 11232−11239.

Cruz, C.N., Pandis, S.N., 2000. Deliquescence and hygroscopic growth of mixed inorganic-organic atmospheric aerosol. Environ. Sci. Technol. 34, 4313−4319.

Deguillaume, L., Leriche, M., Desboeufs, K., Mailhot, G., George, C., Chaumerliac, N., 2005. Transition metals in atmospheric liquid phases: sources, reactivity, and sensitive parameters. Chem. Rev. 105, 3388−3431.

Dick, W.D., Saxena, P., McMurry, P.H., 2000. Estimation of water uptake by organic compounds in submicron aerosols measured during the southeastern aerosol and visibility study. J. Geophys. Res. Atmos. 105 (D1), 1471−1479.

Ding, J., Zhao, P., Su, J., Dong, Q., Du, X., Zhang, Y., 2019. Aerosol pH and its driving factors in Beijing. Atmos. Chem. Phys. 19, 7939−7954.

Dockery, D.W., Cunningham, J., Damokosh, A.I., Neas, L.M., Spengler, J.D., Koutrakis, P., Ware, J.H., Raizenne, M., Speizer, F.E., 1996. Health effects of acid aerosols on north American children: respiratory symptoms. Environ. Health Perspect. 104 (5), 500−505.

Driscoll, C.T., Lambert, K.F., Chen, L., 2007. Acidic deposition: sources and ecological effects // acid in the environment. Springer.

Fang, T., Guo, H., Zeng, L., Verma, V., Nenes, A., Weber, R.J., 2017. Highly acidic ambient particles, soluble metals, and oxidative potential: a link between sulfate and aerosol toxicity. Environ. Sci. Technol. 51 (5), 2611−2620.

Fitriyah, H., Wihandika, R.C., 2018. An analysis of RGB, hue and grayscale under various illuminations. International Conference on Sustainable Information Engineering and Technology (SIET). IEEE, 38–41, doi: 10.1109/SIET.2018.8693160.

Fountoukis, C., Nenes, A., 2007. ISORROPIA II: a computationally efficient thermodynamic equilibrium model for K^+–Ca^{2+}–Mg^{2+}–NH_4^+–Na^+–SO_4^{2-}–NO_3^-–Cl^-–H_2O aerosols. Atmos. Chem. Phys. 7 (17), 4639−4659.

Friese, E., Ebel, A., 2010. Temperature dependent thermodynamic model of the system H^+−NH_4^+−Na^+−SO_4^{2-}−NO_3^-−Cl^-−H_2O. J. Phys. Chem. A. 114 (43), 11595−11631.

Guo, H., Xu, L., Bougiatioti, A., Cerully, K.M., Capps, S.L., Hite Jr, J.R., Carlton, A.G., Lee, S.H., Bergin, M.H., Ng, N.L., Nenes, A., Weber, R.J., 2015. Fine-particle water and pH in the southeastern United States. Atmos. Chem. Phys. 15 (9), 5211−5228.

Guo, H., Liu, J., Froyd, K.D., Roberts, J.M., Veres, P.R., Hayes, P.L., Jimenez, J.L., Nenes, A., Weber, R.J., 2017a. Fine particle pH and gas-particle phase partitioning of inorganic species in Pasadena, California, during the 2010 CalNex campaign. Atmos. Chem. Phys. 17, 5703−5719.

Guo, H., Weber, R.J., Nenes, A., 2017b. High levels of ammonia do not raise fine particle pH sufficiently to yield nitrogen oxide-dominated sulfate production. Sci. Rep. 7, 12109

Guo, H., Nenes, A., Weber, R.J., 2018. The underappreciated role of nonvolatile cations in aerosol ammonium-sulfate molar ratios. Atmos. Chem. Phys. 18 (23), 17307−17323.

Gysel, M., Weingartner, E., Baltensperger, U., 2002. Hygroscopicity of aerosol particles at low temperatures. 2. Theoretical and experimental hygroscopic properties of laboratory generated aerosols. Environ. Sci. Technol. 36, 63−68.

Han, Y., Stroud, C.A., Liggio, J., Li, S.M., 2016. The effect of particle acidity on secondary organic aerosol formation from α-pinene photooxidation under atmospherically relevant conditions. Atmos. Chem. Phys. 16 (21), 13929−13944.

He, K., Zhao, Q., Ma, Y., Duan, F., Yang, F., Shi, Z., Chen, G., 2012. Spatial and seasonal variability of $PM_{2.5}$ acidity at two Chinese megacities: insights into the formation of secondary inorganic aerosols. Atmos. Chem. Phys. 12 (3), 1377−1395.

Hennigan, C.J., Izumi, J., Sullivan, A.P., Weber, R.J., Nenes, A., 2015. A critical evaluation of proxy methods used to estimate the acidity of atmospheric particles. Atmos. Chem. Phys. 15 (5), 2775−2790.

Herrmann, H., Schaefer, T., Tilgner, A., Styler, S.A., Weller, C., Teich, M., Otto, T., 2015. Tropospheric aqueous-phase chemistry: kinetics, mechanisms, and its coupling to a changing gas phase. Chemical reviews. 115 (10), 4259−4334.

Iinuma, Y., Böge, O., Gnauk, T., Herrmann, H., 2004. Aerosol-chamber study of the α-pinene/O_3 reaction: influence of particle acidity on aerosol yields and products. Atmos. Environ. 38 (5), 761−773.

Ito, K., Chasteen, C.C., Chung, H.K., Poruthoor, S.K., Zhang, G.F., Dasgupta, P.K., 1998. A continuous monitoring system for strong acidity in aerosols. Anal. Chem. 70, 2839–2847.

IUPAC: Compendium of Chemical Terminology, 2nd Edn., the “Gold Book”, 1997. http://publications.iupac.org/books/author/mcnaught.html, Accessed date: July 2021.

IUPAC, Solubility Database, 2012. https://srdata.nist.gov/solubility/index.aspx, Accessed date: December 2020.

Jacobson, M.Z., 1999. Studying the effects of calcium and magnesium on size-distributed nitrate and ammonium with EQUISOLV II. Atmos. Environ. 33 (22), 3635−3649.

Jang, M., Czoschke, N.M., Lee, S., Kamens, R.M., 2002. Heterogeneous atmospheric aerosol production by acid-catalyzed particle-phase reactions. Science. 298 (5594), 814−817.

Jang, M., Sun, S., Winslow, R., Han, S., Yu, Z., 2020. In situ aerosol acidity measurements using a UV-visible micro-spectrometer and its application to the ambient Air. Aerosol Sci. Technol. 54 (4), 446−461.

Jia, J., Gao, Y., 2017. Acid deposition and assessment of its critical load for the environmental health of waterbodies in a subtropical watershed, China. J. Hydrol. 555, 155−168.

Jia, S., Sarkar, S., Zhang, Q., Wang, X., Wu, L., Chen, W., Huang, M., Zhou, S., Zhang, J., Yuan, L., Yang, L., 2018a. Characterization of diurnal variations of $PM_{2.5}$ acidity using an open thermodynamic system: a case study of Guangzhou, China. Chemosphere. 202, 677−685.

Jia, S., Wang, X., Zhang, Q., Sarkar, S., Wu, L., Huang, M., Zhang, J., Yang, L., 2018b. Technical note: comparison and interconversion of pH based on different standard states for aerosol acidity characterization. Atmos. Chem. Phys. 18 (15), 11125−11133.

John, W., Hering, S., Reischl, G., Sasaki, G., 1983. Characteristics of nuclepore filters with large pore size−II. filtration properties. Atmos. Environ. 17 (2), 373−382.

Kawakami, N., Osada, K., Nishita, C., Yabuki, M., Kobayashi, H., Hara, K., Shiobara, 2008. Factors controlling sea salt modification and dry deposition of nonsea-salt components to the ocean. J. Geophys. Res. Atmos. 113, D14216.

Koutrakis, P., Wolfson, J.M., Spengler, J.D., 1988. An improved method for measuring aerosol strong acidity: results from a nine-month study in St Louis, Missouri and Kingston, Tennessee. Atmos. Environ. 22 (1), 157−162.

Lawrence, G.B., Hazlett, P.W., Fernandez, I.J., Ouimet, R., Bailey, S.W., Shortle, W.C., Smith, K.T., Antidormi, M.R., 2015. Declining acidic deposition begins reversal of forest-soil acidification in the northeastern U.S. and eastern Canada. Environ. Sci. Technol. 49 (22), 13103−13111.

Lewandowski, M., Jaoui, M., Offenberg, J.H., Krug, J.D., Kleindienst, T.E., 2015. Atmospheric oxidation of isoprene and 1,3-butadiene: influence of aerosol acidity and relative humidity on secondary organic aerosol. Atmos. Chem. Phys. 15 (7), 3773−3783.

Li, Y, Harrison, R.M., 1990. Comparison of indoor and outdoor concentrations of acid gases, ammonia and their associated salts. Environ. Technol. 11 (4), 315−326, doi: org/10.1080/09593339009384868.

Li, J., Jang, M., 2012. Aerosol acidity measurement using colorimetry coupled with a reflectance UV-visible spectrometer. Aerosol Sci. Technol. 46 (8), 833−842.

Li, G., Su, H., Ma, N., Zheng, G., Kuhn, U., Li, M., Klimach, T., Pöschl, U., Cheng, Y., 2020a. Multifactor colorimetric analysis on pH-indicator papers: An optimized approach for direct determination of ambient aerosol pH. Atmos. Meas. Tech. 13 (11), 6053–6065.

Li, M., Weschler, C.J., Bekö, G., Wargocki, P., Lucic, G., Williams, J., 2020b. Human ammonia emission rates under various indoor environmental conditions. Environ. Sci. Technol. 54 (9), 5419−5428.

Lide, D.R., 1994. CRC handbook of chemistry and physics. Vol. 75. CRC press.

Light, T.S., 1984. Temperature dependence and measurement of resistivity of pure water. Anal. Chem. 56 (7), 1138−1142.

Liu, L.J.S., Burton, R., Wilson, W.E., Koutrakis, P., 1996. Comparison of aerosol acidity in urban and semirural environments. Atmos. Environ. 30, 1237–1245.

Liu, H.J., Zhao, C.S., Nekat, B., Ma, N., Wiedensohler, A., Pinxteren, D.V., Spindler, G., Müller, K., Herrmann, H., 2014. Aerosol hygroscopicity derived from size-segregated chemical composition and its parameterization in the North China Plain. Atmos. Chem. Phys. 14 (5), 2525–2539.

Maeda, M., 2000. Application of Pitzer's equations to dissociation of ammonium ion in concentrated aqueous electrolyte solutions, A review. Bulletin of Nagoya Institute of Technology. 52, 23−32

Meng, Z., Seinfeld, J.H., Saxena, P., Kim, Y.P., 1995. Atmospheric gas–aerosol equilibrium: IV. thermodynamics of carbonates. Aerosol Sci. Technol. 23 (2), 131−154.

Mekic, M., Gligorovski, S., 2021. Ionic strength effects on heterogeneous and multiphase chemistry: Clouds versus aerosol particles. Atmos. Envirn. 244, 117911.

Meskhidze, N., Chameides, W.L., Nenes, A., Chen, G., 2003. Iron mobilization in mineral dust: Can anthropogenic SO_2 emissions affect ocean productivity? Geophys. Res. Lett. 30, 21.

Meskhidze, N., Chameides, W.L., Nenes, A., 2005. Dust and pollution: a recipe for enhanced ocean fertilization? J. Geophys. Res. -Atmos. 110, D03301.

Murphy, J.G., Gregoire, P.K., Tevlin, A.G., Wentworth, G.R., Ellis, R.A., Markovic, M.Z., VandenBoer, T.C., 2017. Observational constraints on particle acidity using measurements and modelling of particles and gases. Faraday Discuss. 200, 379−395.

Nenes. A., Pandis, S.N., Kanakidou, M., Russell, A.G., Song, S.J., Vasilakos, P., Weber, R.J., 2021. Aerosol acidity and liquid water content regulate the dry deposition of inorganic reactive nitrogen. Atmos. Chem. Phys. 21 (8), 6023−6033.

Osada, K., Ueda, S., Egashira, T., Takami, A., Kaneyasu, N., 2011. Measurements of gaseous NH_3 and particulate NH_4^+ in the atmosphere by fluorescent detection after continuous air-water droplet sampling. Aerosol Air Qual. Res. 11 (2), 170−178.

Osada, K., Saito, S., Tsurumaru, H., Hoshi. J., 2019. Vehicular exhaust contributions to high NH_3 and $PM_{2.5}$ concentrations during winter in Tokyo, Japan. Atmos. Environ. 206, 218−224.

Pathak, R.K., Louie, P.K.K., Chan, C.K., 2004. Characteristics of aerosol acidity in Hong Kong. Atmos. Environ. 38 (19), 2965-2974.

Pathak, R.K., Wu, W.S., Wang, T., 2009. Summertime $PM_{2.5}$ ionic species in four major cities of China: nitrate formation in an ammonia-deficient atmosphere. Atmos. Chem. Phys. 9 (5), 1711−1722.

Perrino, C., Santis, F.D., Febo, A., 1990. Criteria for the choice of a denuder sampling technique devoted to the measurement of atmospheric nitrous and nitric acids. Atmos. Environ. 24A (3), 617−626.

Petters, M.D., Kreidenweis, S.M., 2007. A single parameter representation of hygroscopic growth and cloud condensation nucleus activity. Atmos. Chem. Phys. 7 (8), 1961−1971.

Pye, H.O.T., Nenes, A., Alexander, B., Ault, A.P., Barth, M.C., Clegg, S.L., Jr., J.L.C., Fahey, K.M., Hennigan, C.J., Herrmann, H., Kanakidou, M., Kelly, J.T., Ku, I., McNeill, V.F., Riemer, N., Schaefer, T., Shi, G., Tilgner, A., Walker, J.T., Wang, T., Weber, R., Xing, J., Zaveri, R.A., Zuend, A., 2020. The acidity of atmospheric particles and clouds. Atmos. Chem. Phys. 20 (8), 4809−4888.

Quinn, P.K., Bates, T.S., Coffman, D., Onasch, T.B., Worsnop, D., Baynard, T., de Gouw, J.A., Goldan, P.D., Kuster, W.C., Williams, E., Roberts, J.M., Lerner, B., Stohl, A., Pettersson, A., Lovejoy, E.R., 2006. Impacts of sources and aging on submicrometer aerosol properties in the marine boundary layer across the Gulf of Maine. J. Geophys. Res.-Atmos. 111, D23s36.

Rafaj, P., Kiesewetter, G., Gül, T., Schöppa, W., Cofalaa, J., Klimonta, Z., Purohita, P., Heyesa, C., Amanna, M., Borken-Kleefelda, J., Cozzi, L., 2018. Outlook for clean air in the context of sustainable development goals. Global Environmental Change, 53, 1−11.

Raizenne, M., Neas, L.M., Damokosh, A.I., Dockery, D.W., Spengler, J.D., Koutrakis, P., Ware, J.H., Speizer, F.E., 1996. Health effects of acid aerosols on north American children: pulmonary function. Environ. Health Perspect. 104 (5), 506−514.

Rengarajan, R., Sudheer, A.K., Sarin, M.M., 2011. Aerosol acidity and secondary organic aerosol formation during wintertime over urban environment in western India. Atmos. Environ. 45 (11), 1940−1945.

Rindelaub, J.D., Craig, R.L., Nandy, L., Bondy, A.L., Dutcher, C.S., Shepson, P.B., Ault, A.P., 2016. Direct measurement of pH in individual particles via Raman microspectroscopy and variation in acidity with relative humidity. J. Phys. Chem. A. 120 (6), 911−917.

Rockland, L.B., 1960. Saturated salt solutions for static control of relative humidity between 5° and 40° C. Anal. Chem. 32 (10), 1375−1376.

Sakamoto, K., Wang, Q.Y., Kimijima, K., Okuyama, M., Mizuno, T., Yoshikado, H., Kaneyasu, N., 1996. Spatial distributions of ambient aerosol acidity in early winter at South-Kanto area, Japan. Environ. Sci. 7, 237−244.

Saxena, P., Mueller, P.K., Kim, Y.P., Seinfeld, J.H., Koutrakis, P., 1993. Coupling thermodynamic theory with measurements to characterize acidity of atmospheric particles, Aerosol Sci. Tech. 19, 279–293.

Seinfeld, J.H., Pandis, S.N., 2016. Atmospheric chemistry and physics: from air pollution to climate change. Hoboken: John Wiley & Sons, Chapter 7.6, 10.5, and 20.4−20.5.

Shi, G., Xu, J., Shi, X., Liu, B., Bi, X., Xiao, Z., Chen, K., Wen, J., Dong, S., Tian, Y., Feng, Y., Yu, H., Song, S., Zhao, Q., Gao, J., Russell, A., 2019. Aerosol pH dynamics during haze periods in an urban environment in China: use of detailed, hourly, speciated observations to study the role of ammonia availability and secondary aerosol formation and urban environment. J. Geophys. Res. Atmos. 124, 9730−9742.

Snider, G., Weagle, C.L., Murdymootoo, K.K., Ring, A., Ritchie, Y., Stone, E., Walsh, A., Akoshile, C., Anh, N.X., Balasubramanian, R., Brook, J., Qonitan, F.D., Dong, J., Griffith, D., He, K., Holben, B.N., Kahn, R., Lagrosas, N., Lestari, P., Ma, Z., Misra, A., Norford, L.K., Quel, E.J., Salam, A., Schichtel, B., Segev, L., Tripathi, S., Wang, C., Yu, C., Zhang, Q., Zhang, Y., Brauer, M., Cohen, A., Gibson, M.D., Liu, Y., Martins,

J.V., Rudich, Y., Martin, R.V., 2016. Variation in global chemical composition of $PM_{2.5}$: emerging results from SPARTAN. Atmos. Chem. Phys. 16 (15), 9629−9653.

Solomon, P.A., Crumpler, D., Flanagan, J.B., Jayanty, R.K.M., Rickman, E.E., McDade, C.E., 2014. US National PM2:5 Chemical Speciation Monitoring Networks-CSN and IMPROVE: Description of networks. J. Air Waste Ma. 64, 1410–1438.

Song, S., Gao, M., Xu, W., Shao, J., Shi, G., Wang, S., Wang, Y., Sun, Y., McElroy, M.B., 2018. Fine-particle pH for Beijing winter haze as inferred from different thermodynamic equilibrium models. Atmos. Chem. Phys. 18 (10), 7423−7438.

Squizzato, S., Masiol, M., Brunelli, A., Pistollato, S., Tarabotti, E., Rampazzo, G., Pavoni, B., 2013. Factors determining the formation of secondary inorganic aerosol: a case study in the Po Valley (Italy). Atmos. Chem. Phys. 13 (4), 1927−1939.

Stumm, W., Morgan, J.J., 1996. Aquatic chemistry: chemical equilibria and rates in natural waters. Canada: John Wiley & Sons, p. 97−103.

Su, H., Cheng, Y., Pöschl, U., 2020. New multiphase chemical processes influencing atmospheric aerosols, air quality, and climate in the Anthropocene. Acc. Chem. Res. 53 (10), 2034−2043.

Surratt, J.D., Lewandowski, M., Offenberg, J.H., Jaoui, M., Kleindienst, T.E., Edney, E.O., Seinfeld, J.H., 2007. Effect of acidity on secondary organic aerosol formation from isoprene. Environ. Sci. Technol. 41 (15), 5363−5369.

Surratt, J.D., Chan, A.W.H., Eddingsaas, N.C., Chan, M., Loza, C.L., Kwan, A.J., Hersey, S.P., Flagan, R.C., Wennberg, P.O., Seinfeld, J.H., 2010. Reactive intermediates revealed in secondary organic aerosol formation from isoprene. Proc. Natl. Acad. Sci. 107 (15), 6640−6645.

Tang, I.N., Munkelwitz, H.R., 1994. Water activities, densities, and refractive indices of aqueous sulfates and sodium nitrate droplets of atmospheric importance. J. Geophys. Res. Atmos. 99 (D9), 18801−18808.

Tanner, R.L., Leaderer, B.P., Spengler, J.D., 1981. Acidity of atmospheric aerosols. Environ. Sci. Technol. 15 (10), 1150-1153.

Tao, Y., Murphy, J.G., 2019. The sensitivity of $PM_{2.5}$ acidity to meteorological parameters and chemical composition changes: 10-year records from six Canadian monitoring sites. Atmos. Chem. Phys. 19, 9309−9320.

Tian, S., Pan, Y., Wang, Y., 2018. Ion balance and acidity of size-segregated particles during haze episodes in urban Beijing. Atmos. Res. 201, 159−167.

Topping, D.O., McFiggans, G.B., Coe, H., 2005. A curved multi-component aerosol hygroscopicity model framework: Part 1 - Inorganic compounds, Atmos. Chem. Phys. 5, 1205−1222.

Vasilakos, P., Russell, A., Weber, R., Nenes, A., 2018. Understanding nitrate formation in a world with less sulfate, Atmos. Chem. Phys. 18, 12765–12775.

Vecchi, R., Valli, G., Fermo, P., D'Alessandro, A., Piazzalunga, A., Bernardoni, V., 2009. Organic and inorganic sampling artefacts assessment. Atmos. Environ. 43 (10), 1713−1720.

Vieira-Filho, M., Pedrotti, J.J., Fornaro, A., 2016. Water-soluble ions species of size-resolved aerosols: implications for the atmospheric acidity in São Paulo megacity, Brazil. Atmos. Res. 181, 281−287.

Vogt, R., Crutzen, P.J., Sander, R., 1996. A mechanism for halogen release from sea-salt aerosol in the remote marine boundary layer. Nature. 383 (26), 327.

Von Bobrutzki, K., Braban, C.F., Famulari, D., Jones, S.K., Blackall, T., Smith, T.E.L., Blom, M., Coe, H., Gallagher, M., Ghalaieny, M., McGillen, M.R., Percival, C.J., Whitehead, J.D., Ellis, R., Murphy, J., Mohacsi, A., Pogany, A., Junninen, H., Rantanen, S., Sutton, M.A., Nemitz, E., 2010. Field inter-comparison of eleven atmospheric ammonia measurement techniques. Atmos. Meas. Tech. 3, 91–112.

Warneck, P., Williams, J., 2012. The atmospheric Chemist's companion: Numerical data for use in the atmospheric sciences. Berlin: Springer Science & Business Media, p.130.

Wang, Y., Zhuang, G., Tang, A., Yuan, H., Sun, Y., Chen, S., Zheng, A., 2005. The ion chemistry and the source of $PM_{2.5}$ aerosol in Beijing. Atmos. Environ. 39 (21), 3771–3784.

Weber, R.J., Guo, H., Russell, A.G., Nenes, A., 2016. High aerosol acidity despite declining atmospheric sulfate concentrations over the past 15 years. Nat. Geosci. 9, 282−285.

Wei, H., Vejerano, E.P., Leng, W., Huang, Q., Willner, M.R., Marr, L.C., Vikesland, P.J., 2018. Aerosol microdroplets exhibit a stable pH gradient. Proc. Natl. Acad. Sci. 115 (28), 7272−7277.

Wexler, A.S., Clegg, S.L., 2002. Atmospheric aerosol models for systems including the ions H^+, NH_4^+, Na^+, SO_4^{2-}, NO_3^-, Cl^-, Br^-, and H_2O. J. Geophys. Res. 107 (D14), 4207.

Whitey, K.T., 1978. The physical characteristics of sulfur aerosols. Atmos. Environ. 12, 135−159.

World Health Organization, 2017. Evolution of WHO air quality guidelines: past, present and future. https://www.who.int/airpollution/ambient/en/

Wu, W., Zhang, Y., 2018. Effects of particulate matter ($PM_{2.5}$) and associated acidity on ecosystem functioning: response of leaf litter breakdown. Environ. Sci. Pollut. Res. 25 (30), 30720−30727.

Xiao, H.W., Xiao, H.Y., Shen, C.Y., Zhang, Z.Y., Long, A.M., 2018. Chemical composition and sources of marine aerosol over the Western North Pacific Ocean in winter. Atmosphere. 9 (8), 298.

Xu, J., Song, S., Harrison, R.M., Song, C., Wei, L., Zhang, Q., Sun, Y., Lei, L., Zhang, C., Yao, X., Chen, D., Li, W., Wu, M., Tian, H., Luo, L., Tong, S., Li, W., Wang, J., Shi, G., Huangfu, Y., Tian, Y., Ge, B., Su, S., Peng, C., Chen, Y., Yang, F., Mihajlidi-

Zelić, A., Đorđević, D., Swift, S.J., Andrews, I., Hamilton, J.F., Sun, Y., Kramawijaya, A., Han, J., Saksakulkrai, S., Baldo, C., Hou, S., Zheng, F., Daellenbach, K.R., Yan, C., Liu, Y., Kulmala, M., Fu, P., Shi, Z., 2020. An interlaboratory comparison of aerosol inorganic ion measurements by ion chromatography: Implications for aerosol pH estimate. Atmos. Meas. Tech. 13, 6325–6341.

Xue, J., Lau, A.K.H., Yu, J.Z., 2011. A study of acidity on $PM_{2.5}$ in Hong Kong using online ionic chemical composition measurements. Atmos. Environ. 45 (39), 7081−7088.

Yao, X., Ling, T.Y., Fang, M., Chan, C.K., 2006. Comparison of thermodynamic predictions for in situ pH in $PM_{2.5}$. Atmos. Environ. 40 (16), 2835−2844.

Zaveri, R.A., Easter, R.C., Fast, J.D., Peters, L.K., 2008. Model for simulating aerosol interactions and chemistry (MOSAIC). J. Geophys. Res. Atmos. 113, D13204.

Zhang, Q., Duan, F., He, K., Ma, Y., Li, H., Kimoto, T., Zheng, A., 2015. Organic nitrogen in $PM_{2.5}$ in Beijing. Front. Environ. Sci. Eng. 9 (6), 1004−1014.

Zhang, Y., Chen, Y., Lei, Z., Olson, N.E., Riva, M., Koss, A.R., Zhang, Z., Gold, A., Jayne, J.T., Worsnop, D.R., Onasch, T.B., Kroll, J.H., Turpin, B.J., Ault, A.P., Surratt, J.D., 2019. Joint impacts of acidity and viscosity on the formation of secondary organic aerosol from isoprene epoxydiols (IEPOX) in phase separated particles. ACS Earth Space Chem. 3 (12), 2646−2658.

Zheng, G., Su, H., Wang, S., Andreae, M.O., Pöschl, U., Cheng, Y., 2020. Multiphase buffer theory explains contrasts in atmospheric aerosol acidity. Science. 369 (6509), 1374−1377.

Zhou, M., Zhang, Y., Han, Y., Wu, J., Du, X., Xu, H., Feng, Y., Han, S., 2018. Spatial and temporal characteristics of $PM_{2.5}$ acidity during autumn in marine and coastal area of Bohai Sea, China, based on two-site contrast. Atmos. Res. 202, 196−204.

Zhou, Y., Xue, L., Wang, T., Gao, X., Wang, Z., Wang, X., Zhang, J., Zhang, Q., Wang, W., 2012. Characterization of aerosol acidity at a high mountain site in central eastern China. Atmos. Environ. 51, 11−20.

Acknowledgements

It has been a precious experience pursuing my PhD study in Nagoya University. I also remember myself as a curious young girl with big smiles when I first stepped into this beautiful campus. Four years has passed and there comes the graduation. I am still curious but my understanding has significantly improved.

I would like to pay special thanks to my parents for their support and encouragement. Because of them, I made up my mind to study in Japan. I would like to express my sincere thanks to my Supervisors, Prof. Kazuo Osada, for his patient guidance, scientific advices as well as continuous encouragement. He always makes time for me in his busy schedule to discuss my research and give the professional comments. His attitude to academic researches gave me a deep impression which is beneficial to my following life. I am also grateful to Prof. Michihiro Mochida and Prof. Urumu Tsunogai for many useful suggestions. Thanks other professors in Graduate School of Environmental Studies as well. I also wish to express gratitude to Dr. Sayako Ueda and Dr. Ippei Nagao for helpful discussions throughout this study. I would like to acknowledge Koki Yamato, Satomi Hirono and Yu Enomoto for atmospheric sampling and chemical analysis. Thanks to the all the members of our research group.

Last but not least, I greatly appreciate Prof. Qiangbin Zhang for the suggestions and encouragements. Thanks to my best friends Dr. Yuqing Da, Walaa Al-Malki, Di Gao, Chen Chen and other friends who encouraged me when I was in something that didn't go smoothly. I would also like to express my special thanks to Japanese Government (Monbukagakusho: MEXT) for supporting the scholarship in those three years which gave me an opportunity to study in Japan.

This study was partly supported by the Environment Research and Technology Development Fund (JPMEERF20165004) of the Environmental Restoration and Conservation Agency of Japan. I also gratefully appreciate Elmar Friese and Adolf Ebel for sharing the E-AIM model (http://www.aim.env.uea.ac.uk/aim/aim.php).

Publications

Song, Q., Osada, K., 2020. Seasonal variation of aerosol acidity in Nagoya, Japan and factors affecting it. Atmospheric Environment. X. 100062.

Song, Q., Osada, K. Direct measurement of aerosol acidity using pH testing paper and hygroscopic equilibrium under high relative humidity. Atmospheric Environment, (Under review)